Turkish Journal of Earth Sciences

Manuscript 1911

Evidence of IOA-IOCG transition ore systems in the Tarom-Hashtjin metallogenic province, NW Iran

MAJID GHASEMI SIANI

Amir Ali Tabbakh Shabani

NURULLAH HANİLÇİ

Franz Neubauer

NAMIK AYSAL

See next page for additional authors

Evidence of IOA-IOCG transition ore systems in the Tarom-Hashtjin metallogenic province, NW Iran

Authors

MAJID GHASEMI SIANI, Amir Ali Tabbakh Shabani, NURULLAH HANİLÇİ, Franz Neubauer, NAMIK AYSAL, and Behrouz Karimi Shahraki

TÜBİTAK

Turkish Journal of Earth Sciences

http://journals.tubitak.gov.tr/earth/

Research Article

Turkish J Earth Sci
(2024) 33: 260-278

doi:10.55730/1300-0985.1911

Evidence of IOA-IOCG transition ore systems in the Tarom-Hashtjin metallogenic province, NW Iran

Majid GHASEMI SIANI[1,*], Amir Ali TABBAKH SHABANI[1], Nurullah HANİLÇİ[2], Franz NEUBAUER[3], Namık AYSAL[2], Behrouz KARIMI SHAHRAKI[1]

[1]Department of Geochemistry, Faculty of Earth Sciences, Kharazmi University, Tehran, Iran
[2]Department of Geological Engineering, Istanbul University-Cerrahpasa, İstanbul, Turkiye
[3]Department of Environment and Biodiversity, Paris-Lodron-University of Salzburg, Salzburg, Austria

Received: 17.02.2023 • **Accepted/Published Online:** 10.01.2024 • **Final Version:** 19.03.2024

Abstract: Kiruna-type iron oxide-apatite (IOA) and iron oxide copper-gold (IOCG) deposits are commonly spatially and temporally associated with one another and coeval host magmatism. The Zanjan area in the Tarom-Hashtjin metallogenic province (THMP) in NW Iran hosts several iron oxide deposits that exhibit a close spatial and temporal relationship with Upper Eocene granitoids. Here, using fluid inclusion, mineralogy, and hydrothermal alteration data from the Chore-Nab iron oxide deposit in combination with other deposits, a new genetic model is developed to explain the formation of the iron oxide mineralization. Furthermore, evidence of an IOA-IOCG transition ore system (IO ± A) in this province is presented. The Chore-Nab orebodies have undergone sodic (albite) alteration associated with an early mineralization stage followed by calcic-sodic (actinolite-rich) alteration related to the formation of a second mineralization stage. The process was finally completed by late veinlets of chalcopyrite, which are related to potassic alteration. Fluid inclusion data show that the initial ore-forming fluids (liquid-vapor- and liquid-vapor-solid)-type inclusions of disseminated ore) have an average temperature and salinity of 403 °C, 14.2 wt.% NaCl equiv., and 371 °C, 44.9 wt.% NaCl equiv., respectively. The temperature and salinity of fluids decreased to an average of 277 °C and 8.9 wt.% NaCl equiv. during the formation of magnetite and magnetite-actinolite veins (LV-type inclusions). Subsequently, the values dropped to an average of 266 °C and 5.3 wt.% NaCl equiv. from late chalcopyrite veinlets (LV-type inclusions). These temperature and salinity values indicate a magmatic-hydrothermal ore system. Dilution and cooling of the hot magmatic-hydrothermal metalliferous fluid by mixing with meteoric fluids may have been the main mechanisms responsible for the deposition of metals transported as metal chloride complexes. A decrease in temperature and apatite content, as well as an increase in Cu content is observed from southeastern Sorkhe-Dizaj deposit (massive magnetite + apatite) to the northwest Chore-Nab deposit in the Zanjan area. The dominant element association in the Chore-Nab deposit (Fe) differs from IOCG (Fe-Cu-Au) and IOA (Fe-P) deposits. These results reveal that IOA deposits (e.g., Sorkhe-Dizaj) were formed along deep-seated crustal faults and ascending fluids, which transported Fe and minor Cu to intermediate levels of the system. Therefore, magnetite and sulfides precipitated to form the Chore-Nab IO ± A deposit. This model explains the transition of IOA-IOCG deposits within the same area, providing a valuable conceptual framework to define further exploration strategies in the Tarom-Hashtjin metallogenic province and elsewhere.

Key words: IOA-IOCG transition, iron oxide mineralization, fluid inclusion, hydrothermal alteration, Zanjan area

1. Introduction

Iron oxide deposits are divided into iron oxide-apatite (IOA) or Kiruna-type and iron oxide-copper-gold (IOCG) deposits. The interest in these deposit systems stems from substantial quantities of magnetite and/or hematite, as well as the varying amounts of Cu, Au, REE, P, U, Ag, and Co (Hitzman et al., 1992; Hitzman, 2000; Barton and Johnson, 2004; Hitzman and Valenta, 2005; Groves et al., 2010; Williams, 2010; Barton, 2014). The two types of deposit are mutually interconnected, forming within the same geographical region and frequently in the same district (Williams et al., 2005). For example, in the Chilean iron belt (Sillitoe, 2003) and Missouri in the United States (Day et al., 2016), IOA deposits exhibit both spatial and temporal associations with IOCG deposits. Analysis of drill core and geophysical data reveals that the spatial relationship is primarily influenced by depth. At shallow paleodepths grades, IOCG mineralization grades into sulfide-poor IOA mineralization with increasing depth. This identification of this structurally controlled, vertical continuum has prompted many scholars to posit that these two deposit types are part of a single, vertically zoned ore-forming system (Sillitoe, 2003; Williams et al., 2005; Simon et al., 2018).

* Correspondence: m.ghasemi@khu.ac.ir

The substantial IOCG and IOA deposits were formed mainly in Precambrian intracratonic settings; while comparatively smaller Phanerozoic deposits formed in relation to convergent margin settings (Sillitoe, 2003; Groves et al., 2010; Simon et al., 2018). Titanium-poor magnetite modally dominates IOA deposits, distinguishing them from nelsonites, whereas magnetite and hematite modally dominate IOCG deposits (Williams et al., 2005). Both deposit types contain metal sulfides, but economic grades are only reached in IOCG deposits.

Iron oxide deposits in Iran formed during the tectono-magmatic evolution related to intracratonic Early Cambrian magmatism in Central Iran and subduction-related Cenozoic magmatism in the Alborz Magmatic Arc (AMA) (Nabatian et al., 2014a) (Figure 1). Additional Cenozoic magmatic belts in Iran comprise the NW-SE trending Urumieh-Dokhtar Magmatic Arc (UDMA) and the Central-East Iran Magmatic Assemblage, which occurs in the hinterland of the Arabian-Eurasia collision zone within the extensive Alpine-Himalayan orogenic belt (Allen et al., 2004). The predominant iron oxide deposits originated in the Bafgh mining area of Central Iran, hosting reserves exceeding two billion tonnes of Fe across more than eighty major magnetic anomalies within a large area of 7500 km^2 (Figure 1a). The Bafgh mining area is dominated by mineral assemblages of low-Ti magnetite-apatite-actinolite, and deposits range in size from large to small (Torab and Lehmann, 2007). Hence, both IOCG and IOA types are hosted by a Lower Cambrian sequence of lavas, pyroclastic and epiclastic rocks, which are intercalated with carbonates and subvolcanic granitoids (Nabatian et al., 2014a). The iron oxide ores commonly contain abundant IOA-type mineralizations containing REE-rich apatite (e.g., Chador-Malu, Esfordi, Se-Chahun, Mishdovan, Chahgaz, Choghart and Lakkeh-Siah) (Daliran, 1990, 1999, 2002; Jami et al., 2007; Torab and Lehmann, 2007; Daliran et al., 2009, 2010; Stosch et al., 2011; Bonyadi et al., 2011; Heidarian et al., 2017). Additionally, IOCG type locally contains significant amounts of Au, Cu, U, Bi, Co (e.g., Jalal-Abad) (Mehrabi et al., 2019).

In addition to the Bafgh mining area, IOA deposits are found within the Cenozoic magmatism of the Tarom-Hashtjin metallogenic province (THMP) in the Alborz-Azarbaijan Magmatic Arc (western section of AMA). These IOA deposits formed along the NW–SE trending magmatic belt in the Zanjan area and include Sorkhe-Dizaj, Aliabad, Morvarid, Golestanabad, and Zaker deposits. These deposits exhibit a close spatial and temporal relation with Upper Eocene granitoids, mainly quartz monzonite intrusions, and are locally hosted by Eocene volcanic-volcaniclastic rocks (Nabatian and Ghaderi, 2013; Nabatian et al., 2014a; Kordian et al., 2020). The iron oxide association with abundant apatite mineralization occurs in the form of veins. Each vein typically contains less than 1000 t of ore in the Zaker deposit, which increases to 400,000 t in the Morvarid and Sorkhe-Dizaj deposits (Nabatian et al., 2014a). The geological features, fluid inclusions, alteration, zoning, geochemistry, and genesis of IOA deposits have been extensively studied by Nabatian et al. (2014a). Recent exploration efforts have led to the discovery of the Chore-Nab deposit in the northwestern part of the Zanjan area, which is currently undergoing thorough and detailed exploration. The characteristics of the Chore-Nab deposit (250,000 t of ore with average grades of 36% Fe and 0.26% Cu) are different from other IOA deposits in the Zanjan area. It is characterized by very low apatite and more abundant actinolite contents compared to the other IOA deposits in the Zanjan area. Furthermore, evidence of Cu mineralization was observed in preliminary field studies. These differences raise questions about the ore genesis of the Chore-Nab deposit and whether this deposit can be regarded as a transition between IOA and IOCG mineralized systems. The second main question is whether the Zanjan area represents a singularity or if there are additional prospective regions existing along the western margin of THMP. Despite its economic importance and the possibility of becoming a mine in the near future, this study aims to investigate the evolution of the Chore-Nab hydrothermal system and the associated Cu mineralization based on the geological characteristics of the iron deposit, the mineralogy of ore zones, and hydrothermal alteration. This investigation is supported by fluid inclusion studies to address these fundamental questions. Integrating these new data with published information from adjacent IOA deposits will provide a better understanding of the geology and genesis of the Chore-Nab deposit, thereby indicating possible evidence of overlap of different mineralization styles in the wider Zanjan area.

2. Geological setting

The 600-km-long and 100-km-wide AMA in northern Iran is divided into western and eastern sections by the N–S Rasht-Takestan Fault. The various bedrock types of the AMA consist of a Paleozoic-Mesozoic passive-margin sedimentary sequence with few volcanic rocks, overlain by Cenozoic volcanic and sedimentary rocks in the southern region (Mirnejad et al., 2010). The Cenozoic successions in the AMA primarily consist of marine and subaerial volcano-sedimentary rocks, which are associated with widespread mafic to felsic lava flows, as well as porphyritic and nonporphyritic shallow intrusions (Aghazadeh et al., 2015). Ore mineralizations in the eastern AMA section include porphyry, IOCG, skarn, manto, Mississippi Valley-type (MVT), and Au, Ag, and base metal-rich epithermal

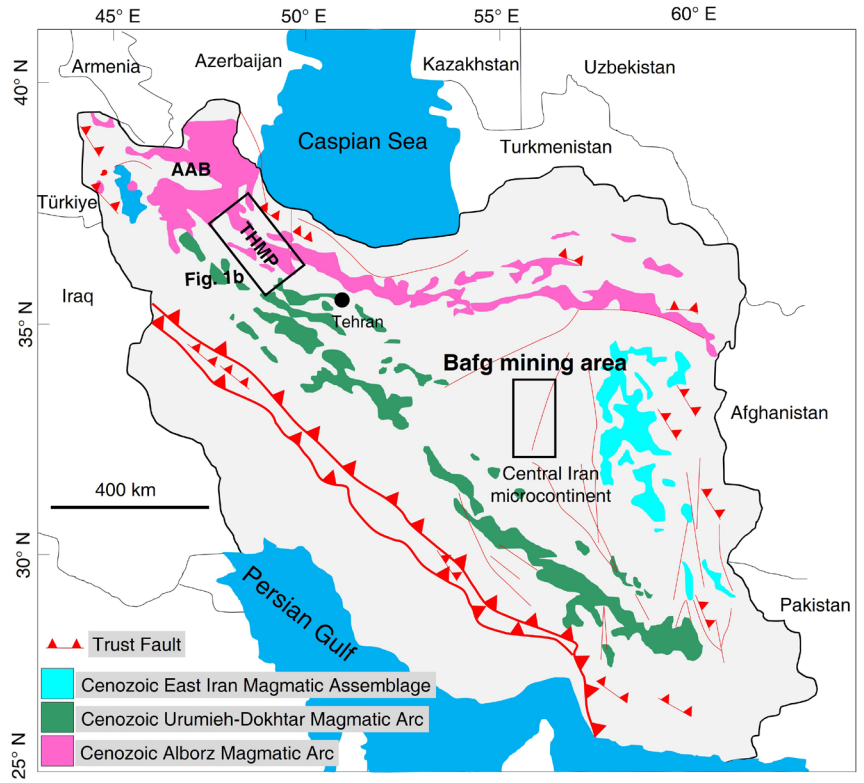

Figure 1. a) Distribution of the Cenozoic magmatism in Iran and Tarom-Hashtjin metallogenic province in the western part of the Alborz Magmatic Arc and location of the Bafgh mining area in Central Iran, and b) geological map of the Tarom-Hashtjin metallogenic province and location of major epithermal ore deposits.

systems, mainly concentrated in the Troud-Chah Shirin belt and adjacent areas, as well as in the eastern part of the AMA (e.g., Shamanian et al., 2004; Mehrabi and Ghasemi Siani, 2012; Mehrabi et al., 2015, 2021; Niroomand et al., 2018; Tale Fazel et al., 2019; Mahdavi Akerdi et al., 2021). In contrast, the western AMA section refers to the Alborz-Azerbaijan magmatic Arc (AAMA) and is highly mineralized, related to numerous granitoid bodies with calc-alkaline to shoshonitic affinity. The AAMA is subdivided into two metallogenic regions, termed the Ahar-Arasbaran metallogenic belt (AAB) in the north and the Tarom-Hashtjin metallogenic province (THMP) in the south (Figure 1a). Numerous epithermal and porphyry ore systems, along with related skarn mineralization types, have formed in relation to several intrusions in the AAB (e.g., Hassanpour et al., 2015). The AAB and THMP extend to the Lesser Caucasus magmatic belt, characterized by dominant porphyry ore mineralization systems (Mederer et al., 2014), as well as skarn and volcanic massive sulfide (VMS) mineralizations (Moritz and Baker, 2019).

The NW-trending THMP is restricted by the extension of the Tabriz-Soltaniyeh and Soltaniyeh-Takestan faults in the southwest and west, the Mianeh Fault in the northwest, and the Astara and Alborz faults in the east (Figure 1b), covering the area between Qazvin (west of Taleghan) and the north-northwest of Mianeh. The THMP is further subdivided into the Tarom belt in the south and Hashtjin belt in the north. The main geological setting within the THMP comprises Eocene pyroclastic rocks (Karaj Formation) and widespread Eocene to Miocene volcaniclastic rocks, including trachybasalt, trachyandesite, trachydacite, andesite, andesitic basalt, basalt, dacite, rhyolitic lava flows, and tuff. The volcaniclastic sequences have been intruded by Upper Eocene intrusions. The Precambrian intrusions, serving as basement, have few outcrops in the THMP. The metallogenic map of the THMP indicates a high concentration of polymetallic low- to high-sulfidation epithermal deposits, along with less common manto-type deposits associated with Eocene to Oligocene volcanic and plutonic rocks in the central and western parts (e.g., Mehrabi et al., 2016; Kouhestani et al., 2020; Ghasemi Siani et al., 2015, 2020; Ghasemi Siani and Lentz, 2022, and references therein). In the eastern part of the THMP, several IOA deposits formed within the Zanjan

area, spatially and temporally accompanied by Zanjan, Zaker, Morvarid, and Kuh-Tabar intrusions (Nabatian et al., 2014a and references therein) (Figure 2).

3. Geology and mineralization of the Zanjan area

The Zanjan area, located in the eastern part of the THMP, is primarily characterized by an extensional phase and Eocene tectonomagmatic activity that includes calc-alkaline to alkaline affinity andesite, as well as widespread andesitic tuff (Karaj Formation) intruded by Upper Eocene intrusions (Figure 2a). Sedimentary rocks such as siltstone, mudstone, and sandstone are associated with the Karaj Formation. The pyroclastic rocks of the Karaj Formation, formed during a period of intense volcanic activity, are classified as the Middle Tuff in the Alborz Mountains (49.3 ± 2.9 Ma), tuffs within the Asara Shale (45.3 ± 2.3 Ma), and Upper tuff (41.1 ± 1.6 Ma) (Verdel et al., 2011). Among the volcanic rocks, andesitic rocks are more widespread and are equivalent to the younger tuff units within the Karaj Formation. Andesitic rocks are the host of the Upper Eocene granitoid intrusions such as those found in Zanjan, Zaker, Morvarid, and Kuh-Tabar in the Zanjan area. They undergo metamorphism (albite-epidote hornfels facies) within the contact aureoles around the granitoid plutons (Nabatian et al., 2014b). These plutons are aligned in NW–SE direction, are concordant with the regional structures, are 3–5 km wide and 22–25 km long, and have an evolved smooth morphology (Nabatian et al., 2014b). Granitoid intrusions covering a compositional range from quartz monzodiorite through quartz monzonite to monzogranite/syenogranite and microquartz diorite are classified as I-type granitoids of calc-alkaline and mostly metaluminous affinity, generated at approximately 40 Ma (Bartonian) in a back-arc tectonic setting (Nabatian et al., 2014b).

The IOA deposits in the Zanjan area are hosted within quartz monzodiorite and quartz monzonite and subordinately by andesitic tuff (Nabatian and Ghaderi, 2013; Nabatian et al., 2013, 2014a). These deposits include Sorkhe-Dizaj in the southeast, Morvarid and Aliabad in the center, and Zaker and Golestanabad in the northwest (Figure 2a). The geochronology of host rocks, alteration, and mineralization in the IOA deposits has been thoroughly studied by Nabatian and Ghaderi (2013), as well as Nabatian et al. (2013, 2014a, 2014b), and is summarized as follows: (1) The Sorkhe-Dizaj IOA deposit consists of low-Ti magnetite with apatite and monazite, along with minor amounts of chalcopyrite, bornite, and pyrite. Additionally, minor to trace amounts of ilmenite and spinel (titanium-magnetite) are present. (2) The main ore body of the IOA Aliabad deposit, 15 to 20 m long, 1 to 2 m thick, consists of vein-type ores of magnetite, associated with gangue minerals such as apatite, diopside, actinolite, phlogopite, chlorite, epidote, quartz, and calcite. (3) The Morvarid IOA deposit comprises several E–W-trending vein-type ore bodies, which are approximately 2–16 m wide, 10–100 m long, and 5–40 m thick, filling fractures and faults. (4) In the Zaker deposit, ore bodies

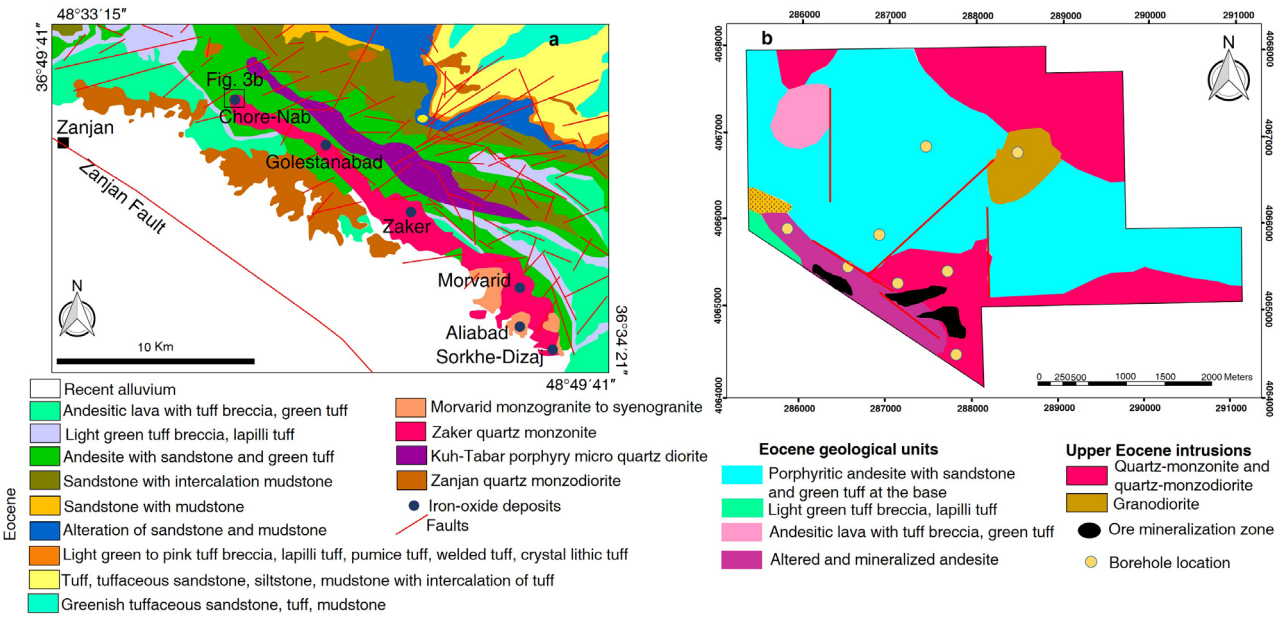

Figure 2. a) Geological map of the Zanjan area in the Tarom-Hashtjin metallogenic province and location of the Chore-Nab deposit and other IOA deposits, and b) geological map of the Chore-Nab deposit.

are 2–7 m wide, up to 600 m long, and 3–15 m thick, trending E–W and dipping 55–65° to the north. The Zaker and Morvarid deposits have the same mineralogy as the Sorkhe-Dizaj and Aliabad deposits, which are characterized by magnetite with abundant apatite (with apatites up to 20 cm long in the Morvarid deposit). (5) The mineralization at Golestanabad is characterized by several NW–SE-trending veins and stockwork-type ore bodies hosted by quartz monzodiorite. The mineralized zones are approximately 20 m wide on average, 20–300 m long, and 1–3 m thick (Kordian et al., 2020). The Chore-Nab deposit is in the far northwestern part of the Zanjan area and will be described in detail in Section 5.

4. Sampling and analytical methods

One hundred and twenty surface and drill core samples from various parts of the Chore-Nab deposit were collected, including samples from mineralized veins, host rocks, iron ores, and hydrothermal alteration zones (Figure 3). Fifty-seven polished thin sections were prepared to study ores and the hydrothermal alteration mineralogy using optical microscopy. In addition, polished samples that were selected underwent examination via electron microprobe (EPMA) using a Cameca SX100 equipped with five WDS spectrometers. The analysis was conducted at the Iranian Mineral Processing Research Center (IMPRC), employing an accelerating voltage of 15 kV and a probe current of 20 nA. The EPMA analyses achieved a detection limit of better than 100 ppm for all elements, due to long integration times on peak and background.

Thirty-two powder samples from hydrothermal alteration zones were analyzed using the X-ray diffraction (XRD) method employing a Philips X′pert model instrument at the IMPRC. The instrument utilized a CoKα1 (1.789Aº) primary beam, a monochronometer on secondary optics, and operated at 40 kV power and 35 mA current. The mineralogical composition of the samples was determined through quantitative XRD spectrometry using the Rietveld method. Data were collected in the range of 4.0 to 80.0 °2θ, with a step size of 0.02°.

Microthermometric measurements were conducted on fluid inclusions identified in seven doubly polished thick sections of quartz and actinolite minerals belonging to magnetite and sulfide mineralizations. The measurements were performed using a Linkam THMS600 freezing-heating stage, which was mounted on a ZEISS Axioplan2 microscope at the IMPRC. The stage was calibrated using cesium nitrate (melting point 414 ºC) and pure water, ensuring a temperature precision of less than ±0.6 ºC for heating and ±0.2 ºC for freezing. During the measurements, the homogenization temperature (T_h), eutectic temperature (T_e), last-ice melting temperature ($T_{m\text{-}ice}$), and $T_{m\text{-}halite}$ values were determined. Salinities in wt.% NaCl equiv. were calculated for halite-bearing inclusions using the equation of Bodnar (1993) for liquid + vapor inclusions, as described by Sterner et al. (1988). based on

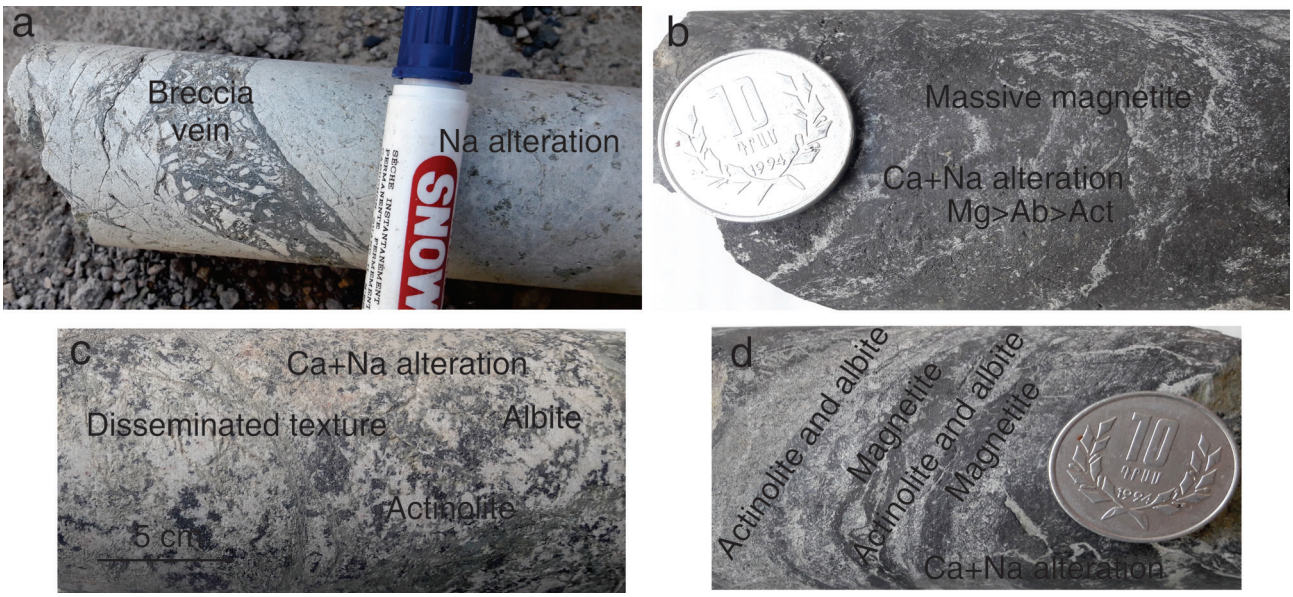

Figure 3. Core samples from the hydrothermal alteration and ore textures at the Chore-Nab deposit: a) breccia vein texture containing magnetite and albite; b) massive ore mineralization associated with calcic-sodic alteration; c) disseminated ore texture showing subhedral to euhedral magnetite associated with actinolite and albite, and d) banded ore textures showing magnetite and actinolite-albite.

5. Chore-Nab deposit

5.1. Deposit geology

The Chore-Nab deposit is in the far northwestern part of the Zanjan area and is hosted by quartz monzonite to quartz monzodiorite (Supplementary Figure 1), as well as by andesitic rocks. It was primarily explored using gravimetry (Supplementary Figure 1a). The main lithotypes identified in the Chore-Nab deposit can be grouped into four categories: (1) porphyritic andesite with sandstone and green tuff, (2) light green tuff breccia and lapilli tuff; (3) andesitic rocks, and (4) intrusive rocks with compositions ranging from quartz monzonite to quartz monzodiorite and granodiorite (Figure 2b). Green porphyritic andesitic rocks consist of plagioclase, hornblende, and less common pyroxene, along with accessory disseminated magnetite, exhibiting microporphyritic and glomeroporphyritic textures. Secondary alteration minerals include chlorite, epidote, and calcite. Andesitic rocks, in some instances, undergo welding and metamorphism upon contact with the plutonic bodies. The quartz monzonite to quartz monzodiorite intrusions display medium- to coarse-grained granular and porphyritic textures, primarily comprising plagioclase, K-feldspar, pyroxene, hornblende, and quartz. Alteration minerals observed include epidote, chlorite, clay minerals, and sericite. Common accessory minerals are magnetite, apatite, and zircon. The frequency of disseminated magnetite increases toward the ore mineralization veins. Ore mineralization is controlled by tectonic processes (faults and fractures) through the ascent of hydrothermal fluids along them. Quartz monzonite to quartz monzodiorite rocks and andesitic rocks undergo alteration along fractures, faults, and around mineralization (Supplementary Figure 1b). Intense hydrothermal alteration and mineralization (Figure 4) are restricted to within several hundred meters across of these fractures and faults.

5.2. Hydrothermal alteration

Field geology, petrographic studies, and XRD analysis indicate seven types of alteration assemblages, including sodic, and calcic-sodic as well as potassic and propylitic alteration. Sericitic (phyllic), silicic, and argillic alteration types are less common in the Chore-Nab deposit (Figure 5). The sodic and calcic-sodic alteration types have developed intensely for up to 40 m around the ore bodies, which host the magnetite mineralization. In general, there is a transition from sodic to calcic-sodic alteration at deeper levels of the deposit. Potassic alteration is observed at intermediate levels within and around sulfide veinlet mineralization, while propylitic alteration typifies the shallow levels. Sodic alteration is associated with breccia textures (Figure 3a) and is characterized by the development of albite associated with magnetite mineralization (Figure 4a). The rock acquires a white color, most prominently observed in the intrusive bodies. The breccia magnetite veins are surrounded by intense sodic alteration (Figure 4b). The earliest hydrothermal sodic alteration grades into zones of pervasive calcic-sodic alteration, which is characterized by massive, acicular fine- to coarse-grained, up to 4 cm long actinolite crystals, intergrown with albite and magnetite ore. The calcic-sodic alteration gives the rock a common light- to dark-green color obtained by both intrusive and andesitic rocks and resulted from the lesser or greater abundance of actinolite and albite that preferably replaced ferromagnesian minerals later replaced by chlorite. The abundance of albite and actinolite varies, with the albite-rich zones observed in the deeper levels, decreasing its proportion towards and close to the vein, where actinolite is abundant. Titanite, pyroxene (diopside), and apatite are observed in the calcic-sodic alteration (Supplementary Figure 2). The calcic-sodic alteration formed with magnetite mineralization, occurring as massive (Figure 3b), disseminated (Figure 3c), and vein-type textures (Figures 5a and 5b), as well as banded mineralization (Figure 3d). Massive magnetite-rich zones contain up to 90% magnetite with a low amount of sulfides associated with albite and actinolite (Figures 4c and 4d). Magnetite ore textures include magnetite veins with lesser amounts of actinolite and albite associated with quartz and calcite (Figure 5a), and magnetite-actinolite veins with minor albite (Figure 5b). Magnetite-actinolite veins are characterized by a higher abundance of magnetite than actinolite and albite at the margin, and by actinolite and albite, with or without magnetite, in the center (Figure 5b). At distances farther from the mineralized zones, extensive formations of actinolite and albite, without magnetite, are observed (Figures 4e and 5c). The sodic and calcic-sodic alteration assemblages are partially overprinted by subsequent potassic alteration, which is structurally controlled by fissures and is observed especially with and around sulfide veinlets (Figure 5d). This alteration is characterized by the presence of K-feldspar (orthoclase), phlogopite, with lesser occurrences of biotite and quartz. However, this type of alteration is poorly developed in the Chore-Nab deposit.

The final stage of alteration is distinguished at surface exposures and is represented by propylitic, with occurrences of sericitic, silicic, and argillic alteration being less common, subsequently overprinted by supergene mineralization. Plagioclase and K-feldspar in the intrusive and volcanic rocks are replaced by clay minerals and sericite. Silicification is in the form of quartz-filled veinlets and vugs within host rocks, overprinting the previous assemblages. Widespread propylitic alteration has developed in the vicinity of mineralized zones along shear zones, lithological contacts, and fracture planes. It is characterized by chlorite-epidote-calcite-quartz

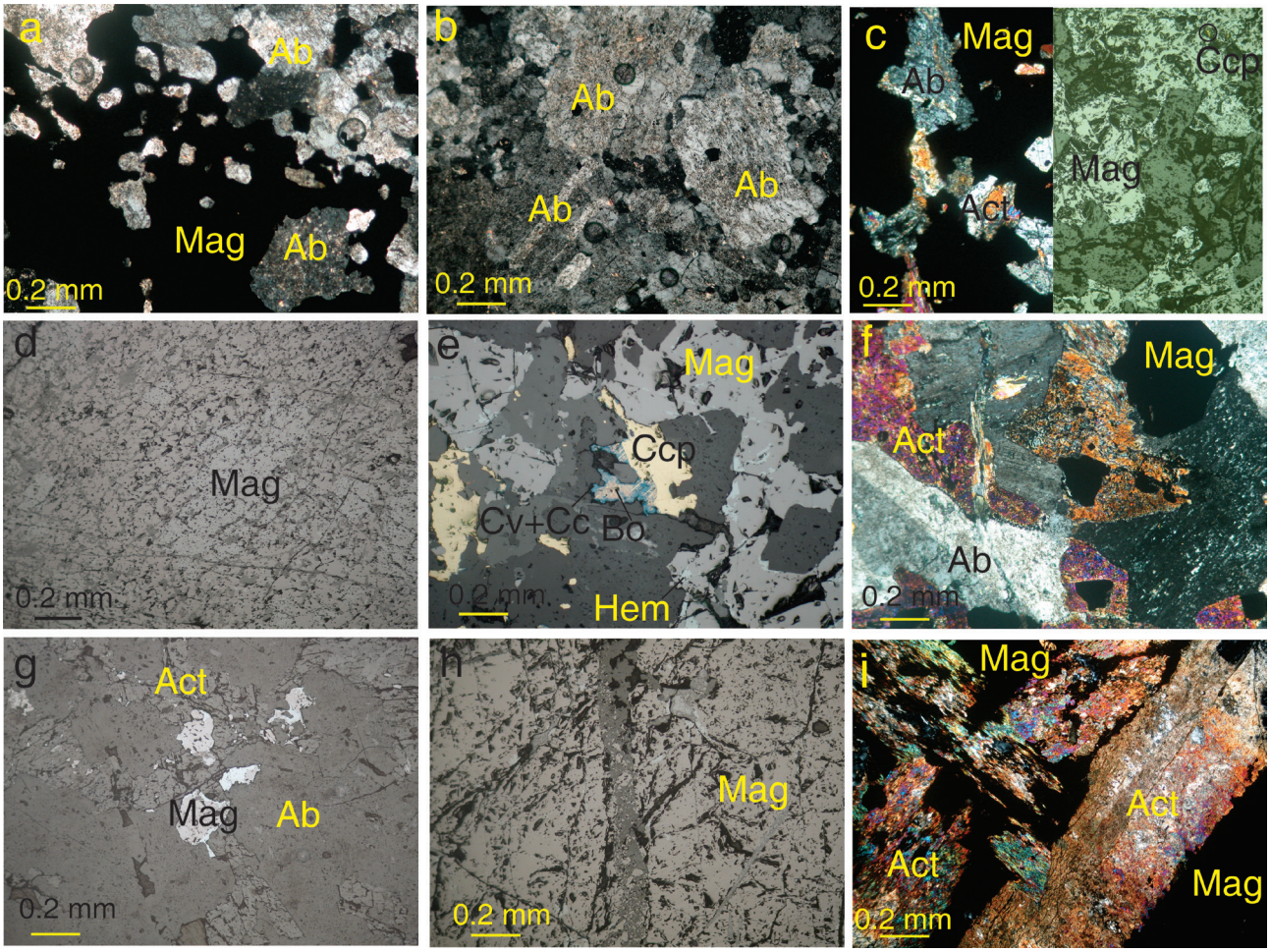

Figure 4. Photomicrographs from the hydrothermal alteration and ores at the Chore-Nab deposit: a) magnetite and albite with a breccia vein texture; b) intense sodic alteration with euhedral coarse-grained albite; c) actinolite associated with massive magnetite mineralization; d) oxidized magnetite to hematite and goethite in the massive magnetite texture; e) chalcopyrite and bornite associated with magnetite in the magnetite vein texture; f and g) subhedral to euhedral magnetite associated with magnetite and albite in the breccia vein texture; h) massive magnetite mineralization, and i) magnetite and actinolite with minor albite at the margin of magnetite-actinolite ore veins. Mag, magnetite; Act, actinolite; Ab, albite; Ccp, chalcopyrite; Bo, bornite; Cc, chalcocite; Cv, covellite.

assemblages. In the altered intrusive and volcanic rocks, chlorite and epidote have replaced pyroxene, actinolite, and plagioclase. In some cases, networks of chlorite and epidote veinlets crosscut the host rock. Dolomite and serpentine group minerals (clinochrysotile) have been detected by XRD in zones of propylitic alteration (Supplementary Figure 3).

5.3. Ore mineralization, paragenetic sequence, and magnetite chemistry

The ore mineralization in the Chore-Nab deposit consists of two outcrops of high-grade, lenticular orebodies (Supplementary Figure 1a). These orebodies comprise breccia, massive, disseminated, and vein-veinlet type ores. Actinolite, albite, epidote, chlorite, orthoclase, phlogopite, muscovite, quartz, pyroxene, apatite, titanite, calcite, and biotite, in order of decreasing abundance, are the main hydrothermal alteration products, which have replaced most primary minerals in these rocks. Pyrite, chalcopyrite, and bornite are the main sulfide minerals. REE-bearing minerals in the titanite and U-Co-Bi-bearing minerals were detected by SEM and EPMA (Supplementary Figure 2). The main mineralized portion occurs as tabular and lens-shaped body characterized by an E–W-trending (N 80–90 E) orientation. It is approximately 0.5–15 m wide, 50–200 m long, and 80–90 m thick (at depth). This ore body is controlled by fractures and fault structures within the interior. The body is predominantly comprised of massive magnetite (≥ 90 vol%), along with varying amounts of actinolite, albite, and sulfide minerals.

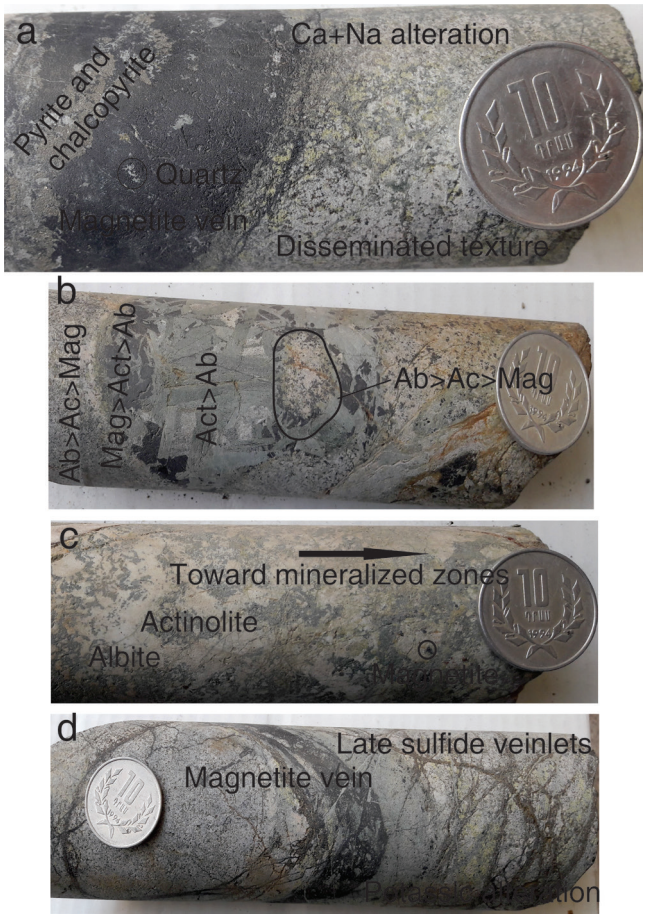

Figure 5. Core samples from the hydrothermal alteration and ore textures at the Chore-Nab deposit: a) magnetite vein texture mainly consisting of magnetite and sulfide; b) magnetite-actinolite ore veins mainly consisting of magnetite and actinolite with minor albite at the margin; c) further ore mineralization, actinolite and albite are the predominant minerals, and d) late chalcopyrite veinlets with potassic alteration.

Disseminated ore mineralization (up to 10 vol%) occurs in the host rocks especially in the surrounding of veins and veinlets. It consists of subhedral to euhedral magnetite and minor pyrite intergrown with other rock-forming and alteration minerals such as quartz, albite, and actinolite (Figures 4f and 4g). A transition is observed from massive magnetite towards intergrowths of magnetite with large actinolite crystals (as veins and veinlets) and albite, leading to disseminated mineralization in the intrusion host rocks containing actinolite and albite. Cu-Fe sulfide mineralization veinlets postdate and overprint the preexisting magnetite mineralization.

A consistent paragenetic sequence of alteration and mineralization can be discerned. The history of alteration and ore mineralization at the Chore-Nab deposit has been divided into four stages: an early breccia-hosted iron oxide stage with sodic alteration; the second stage of magnetite mineralization with massive, disseminated, banded, and vein textures and calcic-sodic alteration; the late stage of chalcopyrite veinlet mineralization with potassic alteration; and finally, the supergene stage (Figure 6). Early mineralized breccias are located in the central portions of disseminated zones or, preferably, along lithological contacts and dilatant structures. These centimeter-sized magnetite breccia veins formed under brittle conditions in the vicinity of massive and disseminated zones and are typically hosted by quartz monzonite, where magnetite formed associated with albite (Figures 4a and 4b). The second stage is characterized by the formation of magnetite and, to a lesser extent, sulfide mineralization, resulting in the development of massive, disseminated, vein, and banded ores. This mineralization

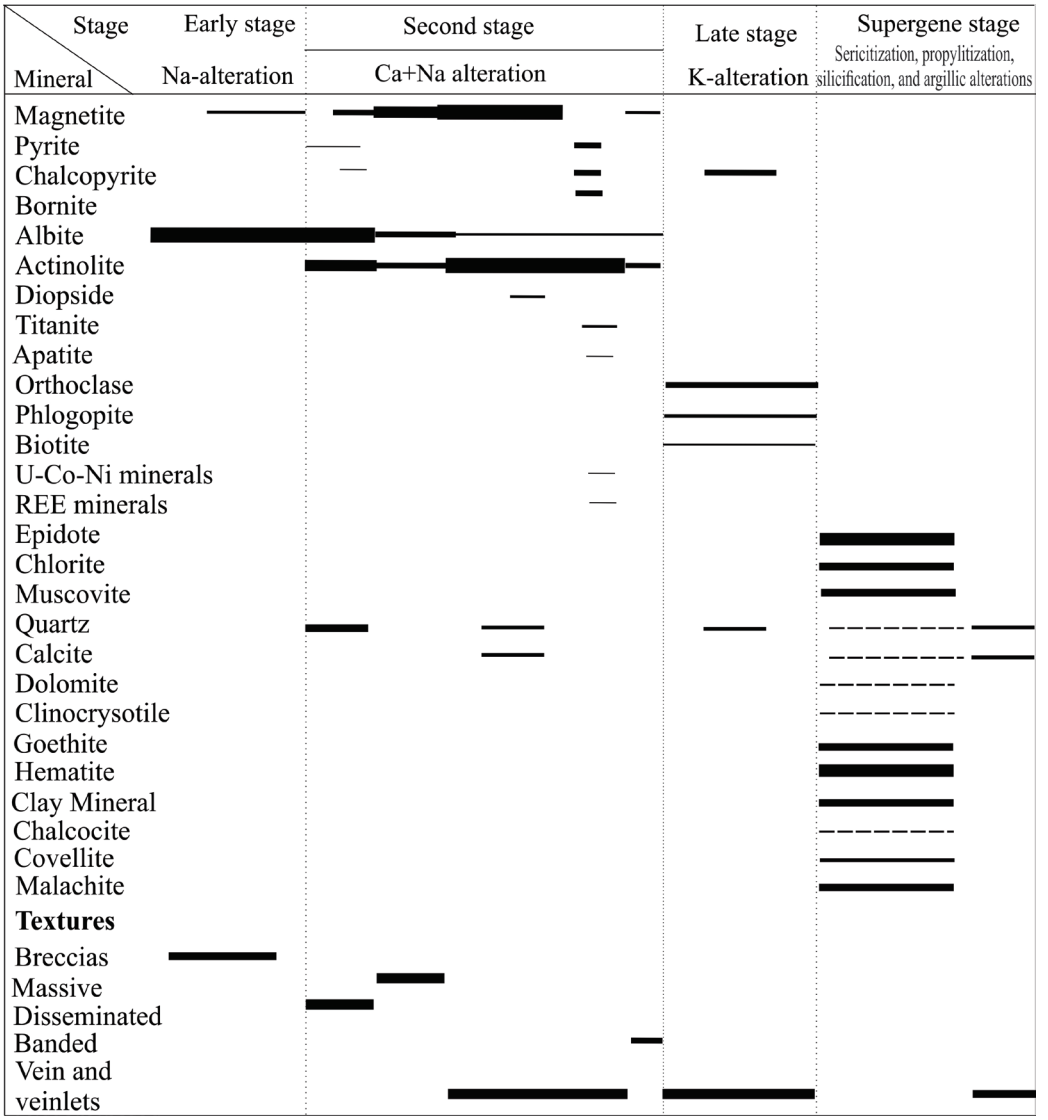

Figure 6. Paragenetic sequence of the hydrothermal alteration and ores based on textures at the Chore-Nab deposit. The thickness of the lines indicates mineral abundance.

is associated with widespread calcic-sodic alteration. The calcic-sodic alteration is pervasive in the country rocks hosting disseminated magnetite mineralization and is characterized by the presence of euhedral to subhedral albite and actinolite grains, along with lesser amounts of quartz, which are observed alongside Ti-bearing magnetite grains (Figures 4f and 4g). EPMA analyses of disseminated magnetite indicate contents of TiO_2 (0.39–0.54 wt.%), V_2O_3 (0.24–0.31 wt.%), CaO (0.01 to 0.02 wt.%), NiO (0.09–0.11 wt.%), Cr_2O_3 (0.03–0.04 wt.%), and MnO (0.03–0.07 wt.%) contents (Table 1). Two types of magnetite ore veins are observed in the Chore-Nab deposit. The first vein type consists of magnetite, chalcopyrite, bornite, and pyrite associated with actinolite, albite, quartz, and calcite (Figures 4e, 4h, and 5a). The second vein type comprises magnetite-actinolite veins containing magnetite and actinolite with minor albite at the margin (Figure 4i), followed by actinolite and albite (Figure 7) with minor magnetite in the middle part (Figure 7a), and finally actinolite and albite without magnetite (with rare pyrite) in the central parts (Figure 7b). REE-bearing titanite (Figure 7b), apatite, and U-Co-Ni-bearing minerals are observed in this type of vein (Supplementary Figures 2a–2d). EPMA analyses of second magnetite mineralization (with a magnetite vein-type texture) reveal significant variations in Ti and V contents among different types of Fe-oxide. These analyses indicate the contents of TiO_2 (0.04–0.08 wt.%), V_2O_3 (0.08–0.13 wt.%), CaO (0.01–0.04

Table 1. Results of electron microprobe analyses of magnetite from the Chore-Nab ore deposit.

Point. No	Disseminated-type magnetite			Vein-type magnetite							
SiO_2	0.02	0.05	0.05	0.07	0.12	0.12	0.19	0.42	0.17	0.06	0.04
TiO_2	0.44	0.54	0.39	0.05	0.05	0.04	0.05	0.05	0.08	0.05	0.07
Al_2O_3	0.07	0.05	0.06	0.05	0.06	0.06	0.01	0.02	0.08	0.06	0.1
Cr_2O_3	0.04	0.04	0.03	0.08	0.03	0.07	0.01	0.02	0.02	0.01	0.01
Fe_2O_3	68.56	68.49	69.87	69.73	69.61	67.95	68.14	68.15	66.46	69.58	67.04
FeO	30.24	30.35	29.15	30.12	29.47	30.95	30.72	31.34	32.24	30.45	32.18
MnO	0.05	0.07	0.03	0.05	0.07	0.04	0.09	0.05	0.04	0.05	0.02
MgO	b.d	0.02	0.02	0.03	0.07	0.06	0.01	0.04	0.06	0.05	0.03
CaO	0.01	0.02	0.01	0.01	0.01	0.02	0.04	0.04	0.01	0.01	0.01
Na_2O	b.d	b.d	0.05	0.01	0.10	0.04	0.05	0.04	b.d	b.d	0.07
K_2O	b.d	b.d	b.d	b.d	b.d	0.06	b.d	b.d	b.d	b.d	b.d
V_2O_3	0.24	0.31	0.31	0.12	0.13	0.11	0.13	0.11	0.12	0.11	0.08
NiO	0.09	0.11	0.09	0.12	0.15	0.16	0.12	0.07	0.08	0.12	0.06
Total	99.76	100.05	100.06	100.44	99.87	99.68	99.56	100.35	99.36	100.55	99.71

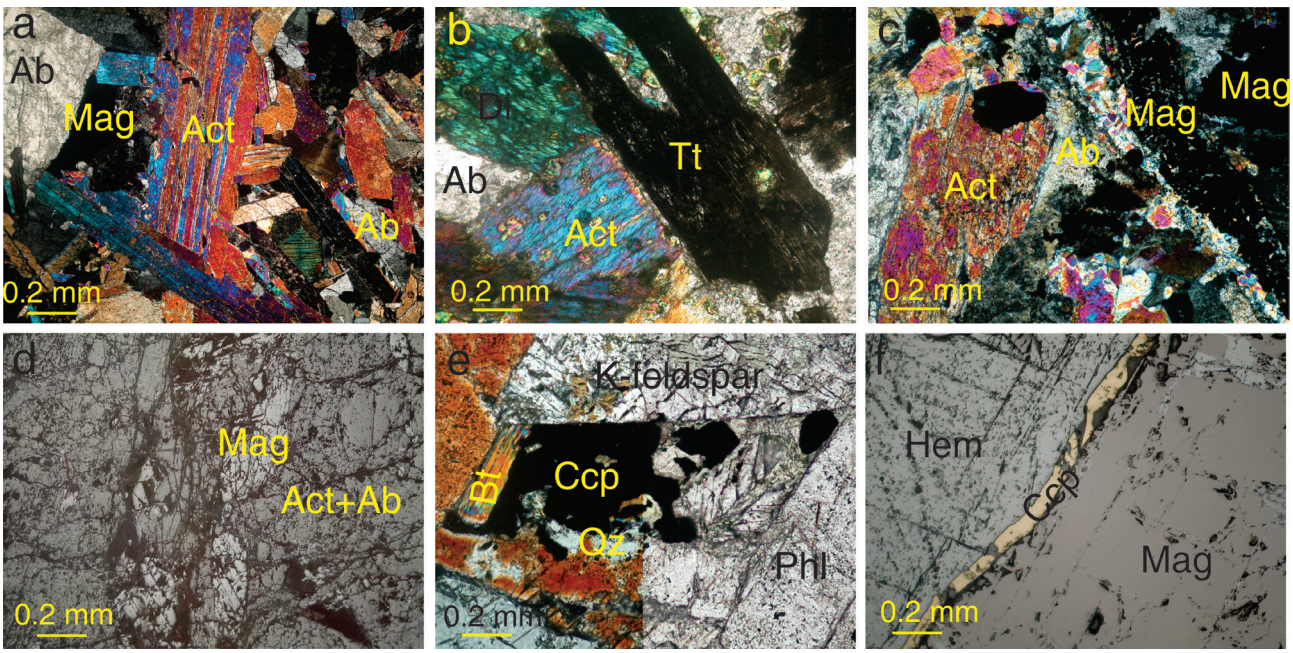

Figure 7. Photomicrographs from the hydrothermal alteration and ores at the Chore-Nab deposit: a) increasing amount of albite with actinolite at the middle part of magnetite-actinolite veins; b) REE-bearing titanite at the center part of magnetite-actinolite veins; c and d) magnetite associated with actinolite-albite at the banded ore textures; e) chalcopyrite mineralization associated with potassic alteration, and f) the mm-sized veinlets of chalcopyrite in close neighborhood to the second stage of magnetite mineralization. Mag, magnetite; Act, actinolite; Ab, albite; Ccp, chalcopyrite; Hem, hematite; Phl, phlogopite; Bt, biotite; Di, diopside; Qz, quartz; Tt, titanite.

wt.%), NiO (0.07–0.16 wt. %), Cr_2O_3 (0.01–0.08 wt.%), and MnO (0.02–0.09 wt.%) (Supplementary Figures 2e and 2d; Table 1). In the banded ore, magnetite formed at the end of the second stage and contains alternating bands of magnetite and actinolite-albite (Figures 7c and 7d). The late Cu-bearing stage is characterized by chalcopyrite veinlets associated with orthoclase, phlogopite, biotite, and minor quartz (Figure 7e). Veinlets of chalcopyrite, measuring millimeters in size, are observed in close association to the second stage of magnetite mineralization (Figure 7f). During the supergene stage, chalcopyrite and bornite minerals were replaced by covellite and chalcocite along their rims and fractures. Additionally, hematite (martitization) formed as a supergene mineral due to magnetite oxidation, predominantly occurring near the surface and along fractured zones. Malachite, goethite, and other hydrous Fe-oxide minerals have developed on the surface within the oxidation zone.

6. Petrography and microthermometric properties of fluid inclusions

Samples for fluid inclusion analysis were collected from disseminated magnetite ore, magnetite veins (second stage), and late chalcopyrite veinlets (late stage) selected from drill cores. Primary, pseudosecondary, and secondary inclusion assemblages (FIAs) were identified according to the criteria of Roedder (1984) and Goldstein (2003). Microthermometric measurements were performed on primary FIAs, which developed in clusters, along growth zones, and in isolations within hydrothermal quartz and actinolite minerals, yielding 62 homogenization temperatures (T_h -°C) and last ice melting ($T_{m\text{-}ice}$) data (Table 2).

Two types of fluid inclusions have been defined by petrographic studies, taking into account the number and proportions of phases present at room temperature (Nash, 1976) (Supplementary Figure 4). These are: (i) halite-bearing inclusions (LVS-type, liquid-vapor-solid) and (ii) two-phase, liquid-rich inclusions (LV-type, liquid-vapor). LVS-type inclusions show irregular and elongated shapes ranging in size from 7 to 12 μm, containing three phases: liquid, vapor, and solid (halite). They commonly exhibit richness in the liquid phase, with a vapor bubble occupying 5 to 25 vol% at room temperature. LVS-type inclusions in quartz are distributed within disseminated magnetite ore of the second stage of the ore mineralization. LV-type inclusions, ranging in size from 5 to 17 μm in quartz and 5 to 9 μm in actinolite, comprise two phases (liquid + vapor), with the dominant liquid phase at room temperature and the vapor phase occupying 5 to 25 vol% of the inclusions. The eutectic temperature (Te) of LV-type inclusions varies from 20.9 to –22.2 °C. The shape of LV-type inclusions ranges from irregular to rounded to elliptical. This type of inclusion is distributed in quartz of magnetite veins, actinolite in magnetite-actinolite veins of the second ore mineralization stage, and finally in quartz of late sulfide veinlets (Supplementary Figure 5).

In eight LVS-type inclusions in quartz, halite crystals melted at temperatures ranging from 300 to 380 °C, and the salinities of these inclusions were calculated to range from 37.9 to 45.1 wt.% NaCl equiv. (Supplementary Figure 5a), based on Sterner et al. (1988). Homogenization of these inclusions occurred in the liquid phase at temperatures ranging from 470 to 510 °C (Supplementary Figure 5b). In thirteen LVS-type inclusions in quartz, the inclusions were homogenized to the liquid phase through the disappearance of halite crystals at temperatures ranging from 334 to 412 °C, corresponding to salinities of 41.4 to 49.2 wt.% NaCl equiv. The vapor of these inclusions disappeared between 301 and 362 °C prior to complete homogenization. The T_h for LV-type fluid inclusions in quartz (n = 18) of the disseminated ore is in the range of 337 to 490 °C (Supplementary Figure 5b) with salinities of 12.3 to 16.3 wt.% NaCl equiv. (Supplementary Figure 5a), with $T_{m\text{-}ice}$ values ranging from –12.4 to –8.6 °C. The LV-type fluid inclusions in the quartz (n = 10) of the magnetite vein ore are characterized by T_h in the range of 268 to 306 °C (average 287.5 °C), with $T_{m\text{-}ice}$ values ranging from –9.6 to –4.5 °C, corresponding to salinities of 7.1 to 13.5 wt.% NaCl equiv. (average 10.3%). The T_h values for LV-type fluid inclusions (n = 7) in the actinolite of the magnetite-actinolite vein are in the range of 250 to 273 °C (average 262 °C) with $T_{m\text{-}ice}$ values ranging from –6.8 to –2.4 °C, corresponding to salinities of 4 to 10.2 wt.% NaCl equiv. (average 6.9%). The T_h values for LV-type fluid inclusions in quartz (n = 6) of the late chalcopyrite veinlet are in the range of 259 to 276 °C (average 265 °C), with $T_{m\text{-}ice}$ values of these type inclusions ranging from –4 to –3.2 °C, corresponding to salinities of 5.2 to 6.4 wt.% NaCl equiv. (average 5.9%).

7. Discussion

The Chore-Nab deposit in northwestern Iran is hosted in NW–SE trending Upper Eocene monzonitic rocks in the Zanjan area, where several iron-oxide deposits occur, such as Moravid, Zaker, Aliabad, Golestanabad, and Sorkhe-Dizaj. Scientific debates regarding the relationship and origin of different classes of iron-oxide-copper-gold deposits (e.g., IOA, IOCG) still continue (i.e. Hitzman, 2000; Sillitoe, 2003; Smith et al., 2007). However, it is well known that the hydrothermal fluids responsible for the formation of such deposits exhibit high salinity and a highly complex chemical composition (i.e. Oliver et al., 2004; Pollard, 2006). Geologic and microthermometric data of fluid inclusions, as well as

Table 2. Fluid inclusion data from Chore-Nab ore deposit: homogenization temperature to liquid (Thl); ice melting temperature (Tm_{ice}); halite melting temperature (Tm_{Halite}); number of analyses (n).

Inclusion type	Host mineral	Mineralization stage	Tm ice (°C)	Tm_{Halite}	Th (°C)	Salinity(wt.% NaCl)
LVS-type	Quartz (n=21)	Disseminated ore	-----	300–412	301–510	37.95–49.21
LV-type	Quartz (n=18)	Disseminated ore	–8.6 to –12.4	-----	337–490	12.39–16.33
LV-type	Quartz (n=10)	Magnetite vein	–4.5 to –9.6	-----	268–306	7.16–13.51
LV-type	Actinolite (n=7)	Magnetite-actinolite vein	–2.4 to –6.8	-----	250–273	4.02–10.23
LV-type	Quartz (n=6)	Late sulfide veinlet's	–3.2 to –4	-----	259–276	5.26–6.44

associated alteration mineral assemblages for the Chore-Nab deposit and other associated iron oxide deposits in the Zanjan area of THMP, have been synthesized to develop the following new conceptual model for these mineralizing systems (Figure 8).

7.1. Geology and mineralogy framework

Iron oxide deposits in the Zanjan area can be placed within a vertically zoned conceptual framework. In this framework, the high-temperature, magnetite IOA deposits, which are rich in massive apatite (Sorkhe-Dizaj, Morvarid, Zaker, and Aliabad deposits), were emplaced at moderate depths (approximately 1–2.5 km). Conversely, magnetite-dominant veins and IO ± A deposits (including the Golestanabad and Chore-Nab deposits) were emplaced at shallow depths. The mineralization temperature decreases from Sorkhe-Dizaj at deeper levels to Chore-Nab deposit at the shallower levels from southeast to northwest of the Zanjan magmatic area (see subsection 7.3). The mineralization in the Chore-Nab deposit is multistage and includes breccia-hosted magnetite veins, disseminated magnetite ores, massive magnetite orebodies, magnetite-actinolite veins, and banded magnetite and chalcopyrite veinlets. Ore mineral assemblages, metal endowments, and alteration assemblages of iron oxide deposits at the Zanjan area systematically vary with depth, indicating that the iron oxide hydrothermal systems were emplaced at diverse crustal depths, resulting in distinctly different mineral assemblages (Figure 8). These include: (1) deep-seated, high-temperature magmatic ± hydrothermal IOA systems, and (2) shallower IO ± A deposits. The IOA deposits (Sorkhe-Dizaj, Morvarid, Zaker, and Aliabad deposits) are magnetite-dominant with a high content of massive apatite and contain less actinolite associated with very minor chalcopyrite, whereas the IO ± A deposits (Golestanabad and Chore-Nab deposits) are characterized by magnetite dominance with minor apatite and abundant

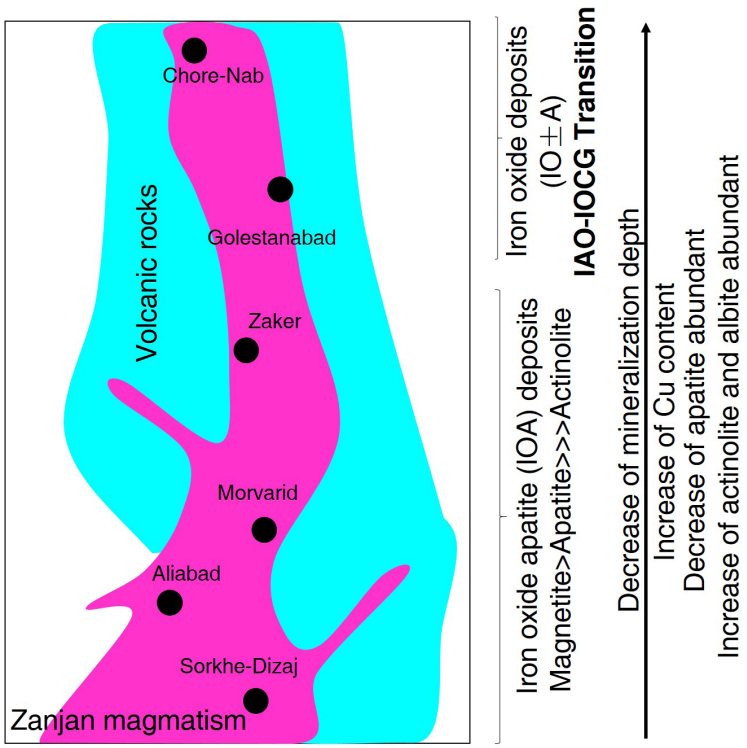

Figure 8. Schematic genetic model (not to scale) for the Upper Eocene magmatism Zanjan area and related iron oxide deposits. This genetic model presented by a distinct vertical transition from Kiruna-type IOA mineralization at depth (Sorkhe-Dizaj, Aliabad, Morvarid, and Zaker) toward IO ± A (could be considered as IOA-IOCG transition) (Golestanabad and Chore-Nab deposits) and typical magnetite-rich IOCG mineralization at intermediate levels, and hematite-rich IOCG mineralization at the shallowest level of the system; the two later types of ore deposits did not form in the Zanjan area; therefore, they are not shown in this model.

actinolite, as well as higher Cu contents. Additionally, the composition of magnetite in the disseminated magnetite ores of Chore-Nab deposit (Supplementary Figure 6) is similar to magnetite compositions of Sorkhe-Dizaj, Morvarid, Zaker, and Aliabad IOA deposits. Conversely, the composition of magnetite in magnetite veins overlaps with that found in IOA and IOCG mineralizations (Dupuis and Beaudoin, 2011) (Supplementary Figure 6).

7.2. Ore-related alteration types

The alteration mineral assemblages in the Zanjan area iron oxide deposits vary according to depth and the type of mineral deposit. Deeper IOA systems (e.g., Sorkhe-Dizaj, Morvarid, Zaker and Aliabad deposits) (Figure 8) are typically spatially associated with calcic alteration halos adjacent to or near magnetite ores. These halos are characterized by abundant massive apatite and tabular actinolite that accompany quartz and magnetite assemblages (Nabatian et al., 2014a). These alteration assemblages and their correlation with depth and inferred equilibrium temperature are similar to findings from several studies on IOA deposits (Day et al., 2016 and references therein). The calcic alteration zones represent partial to complete replacement of the host volcanic rocks by metasomatic fluids associated genetically with the IOA systems. Sodic alteration zones are known to be spatially associated with IOA and IOCG deposits worldwide (e.g., Williams et al., 2005; Barton, 2014). The Chore-Nab orebodies display a consistent pattern of early regional sodic alteration (albite), followed by calcic-sodic alteration (actinolite–albite), which is associated with minor titanite and apatite. Calcic-sodic alteration in the Chore-Nab deposit was followed by potassic alteration associated with late chalcopyrite veinlets and then by the widespread propylitic-sericitic-argillic-silicic alteration types. Sodic alteration developed in early breccia veins as well as in disseminated magnetite ores, and abundant actinolite is a possible transition between sodic and calcic-sodic alteration zones. Calcic-sodic alteration is associated with massive and vein magnetite. Towards the end of the calcic-sodic alteration, the magnetite content decreased, and actinolite-albite content increased. Subsequently, a new mineralization stage (late stage) emerges, generating the chalcopyrite veinlets with the potassic alteration that affected the host rocks. Potassic alteration is more common in the IOCG and IOA-IOCG transition ore systems (Corriveau et al., 2016).

The volcaniclastic and granitoid host rocks are affected by brittle zones, resulting in the development of cataclastic and mylonitic textures. The dominant brittle zones allowed for the precipitation of sodic-calcic minerals mainly within breccias and veins. Following the formation of most magnetite, chalcopyrite began to precipitate as crosscutting veinlets under brittle conditions. During the propylitic-sericitic-argillic-silicic alteration stages, the chlorite-epidote-calcite-quartz assemblage tends to be associated with dilatant structures, indicating a dominantly brittle regime throughout the evolution of the hydrothermal system.

7.3. Evolution of mineralizing fluids

Fluid inclusion data indicate that the disseminated magnetite ore in the Chore-Nab deposit is the initial ore phase formed by fluids with higher temperature and salinity, potentially indicating a magmatic-hydrothermal origin (Supplementary Figure 5). The fluids responsible for the formation of disseminated ore phase are characterized by the LV- and LVS-type inclusions, exhibiting an average T_h of 403 °C (ranging from 337 to 490 °C) and a salinity of 14.2 wt.% NaCl equiv., and a T_h of 371 °C (ranging from 300 to 510 °C) and a salinity of 44.9 wt.% NaCl equiv., respectively (Figure 9). In this ore type, some of the halite-bearing (LVS-type) fluid inclusions were homogenized through the disappearance of halite crystals as the final phase, occurring between 334 and 412 °C. This corresponds to salinities of 41 wt.% NaCl equiv. and 49 wt.% NaCl equiv., respectively. The homogenization through the disappearance of halite crystals is commonly observed in certain hydrothermal deposits, such as porphyry copper, skarn, and IOA/IOCG deposits (e.g., Niiranen et al., 2007; Becker et al., 2008). Pressure and bulk density of these inclusions were identified according to Lecumbberri Sanchez et al. (2012) using microthermometric data of $T_{m\text{-halite}}$ and $T_{hL\text{-}V}$ (Figure 10). Based on the fluid inclusions data (Figure 10), it is estimated that LVS-type inclusions, in which homogenization occurred due to halite disappearance, were trapped at a minimum pressure of 45 MPa (at T_h = 334 °C), which is corresponding to a depth of 1.7 km based on the lithostatic pressure gradient (assuming a density of $\rho = 2.7$ g/cm^3).

The fluid inclusion data from the Chore-Nab deposit indicate that the fluids have higher temperature and salinity during the formation of the disseminated magnetite ore stage. Specifically, temperatures ranged from 337 to 490 °C with 12.3 to 16.3 wt.% NaCl equiv. for the initial ore-forming stage of the LV-type, and from 301 to 510 °C with 37.9 to 49.2 wt.% NaCl equiv. for the LVS-type. The temperature decreased during the formation of magnetite-actinolite veins (from 250 to 306 °C with 4 to 13.5 wt.% NaCl equiv.), and subsequently during the formation of sulfide veins (from 259 to 276 °C with 5.2% to 6.4 wt.% NaCl equiv.; Figure 9). Fluid inclusion data from magnetite-actinolite and late sulfide veins, representing the latest stage of ore formation, show similarities and are distributed within a narrow range. This data reveals that later hydrothermal solutions were responsible for the formation of sulfides and associated gangue minerals.

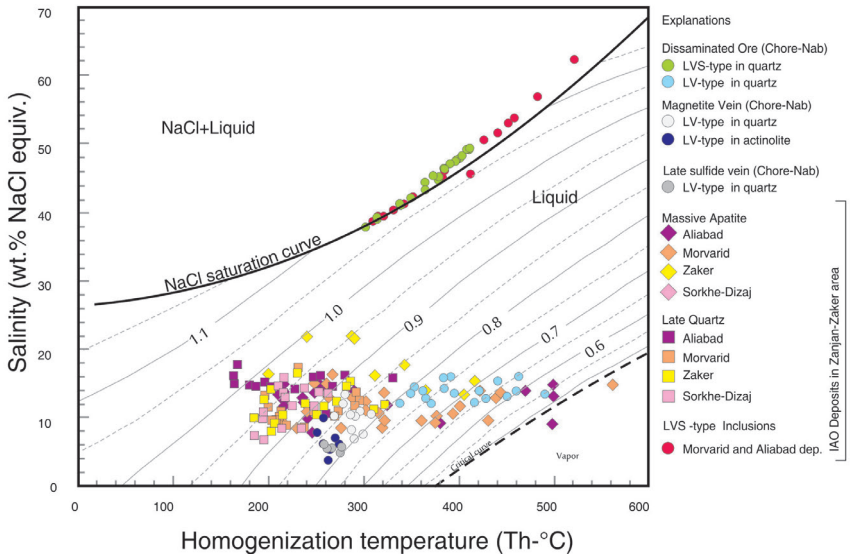

Figure 9. The fluid inclusion homogenization temperature versus salinity diagram indicates the physicochemical processes and temperature and salinity changes during ore mineralization. Data for other IOA deposits in the Zanjan area are from Nabatian et al. (2014a).

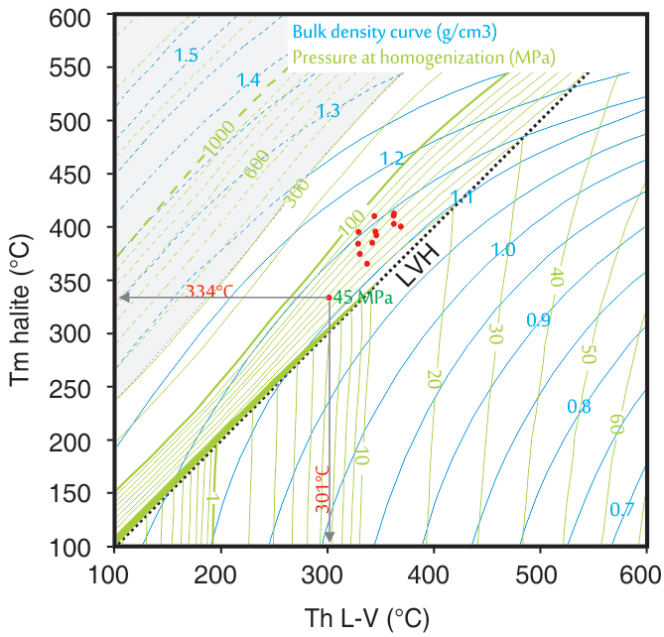

Figure 10. Tm-halite versus Th L-V plots show pressure and bulk density relationships of LVS-type fluid inclusions, in which homogenization occurs with the disappearance of the halite crystal. According to the lowest Tm-halite (334 °C) value, the trapping pressure of these type of inclusions have been estimated at least 45 MPa. The bulk density of fluid (g/cm^3; blue lines), and the pressure (MPa; green lines) are taken from Lecumbberri-Sanchez et al. (2012). The bold dashed line indicates the liquid-vapor-halite (LVH) curve.

At regional scale, there is a decreasing temperature observed from the massive apatite ore of Sorkhe-Dizaj (ranging from 520 to 290 °C with an average of 345 °C) to Morvarid (ranging from 560 to 212 °C with an average of 337 °C), then to Zaker (ranging from 416 to 200 °C with an average of 315 °C) in the southeast to northwest direction of the Zanjan magmatic area, and finally to Aliabad at the margin (with an average temperature of 304 °C) (Nabatian et al., 2014a). Three models have been proposed for IOA/ICOG deposits, involving magmatic-hydrothermal fluid, nonmagmatic fluid (basin derived, meteoric, and metamorphic fluids), and hybrid types (Barton and Johnson, 2004). The high temperature and high salinity of fluid inclusions, along with the presence of halite daughter crystals in fluid inclusions within both apatite and quartz, and stable isotope data (Nabatian et al., 2013), indicate that magmatic-hydrothermal fluids are dominant in the formation of the Zanjan area IOA deposits. The higher temperatures and hypersaline fluids have been formed by magmatic-hydrothermal solutions with high salinity and temperature, remaining after the crystallization of quartz monzonitic composition at high temperatures (up to 510 °C). Subsequently, LV-type fluid inclusions with lower temperatures were accompanied by cooling from 510 to 250 °C due to the mixing of the early, hot magmatic-hydrothermal fluids with meteoric water.

7.4. Ore genesis and model

The magnetite associated with abundant apatite in replacement ore bodies and associated alteration at the Sorkhe-Dizaj, Morvarid, Zaker, and Aliabad deposits classifies them as IOA deposits (Nabatian et al., 2014a). However, the Chore-Nab deposit in the Zanjan area has different mineralogical and geological features compared to the abovementioned IOA deposits. The hydrothermal system at the Chore-Nab displays a complex alteration and mineralization sequence, characterized by early sodic alteration, main calcic-sodic alteration, potassic alteration, and regional propylitic alteration zones. The alteration sequence generally aligns with the alteration zoning predicted in IOCG systems (Hitzman et al., 1992). The late chalcopyrite mineralization is similar to the late hydrothermal alteration sequence observed in other IOCG systems, where the Cu–Au mineralization occurs subsequent to the main iron oxide stage (Marschik and Fontboté, 2001; Edfelt et al., 2005; Mark et al., 2006; Rieger et al., 2010; Reid, 2019). The absence of massive apatite within magnetite mineralization, the lack of REE enrichment, and the abundant actinolite associated with magnetite, as well as occurrences of Cu, Ni, Co, and U mineralization at the Chore-Nab are more similar to IOCG deposits rather than IOA. However, evidence such as uneconomic gold and low volume of Cu-mineralization differentiate it from the classical IOCG deposits. In addition, most magnetite ore is hosted by quartz monzonite to quartz monzodiorite as well as andesitic rocks, whereas most IOCG deposits formed contemporaneously with igneous bodies and are hosted in metavolcanic and sedimentary rocks (Hitzman et al., 1992; Hitzman, 2000; Williams and Pollard, 2003; Hart et al., 2004; Williams et al., 2005; Pollard, 2006; Monteiro et al., 2008; Groves et al., 2010; Williams, 2010; del Real et al., 2021). Mineralogy, fluid inclusion, hydrothermal alteration, and geological field data at the Chore-Nab deposit can potentially support a genetic link between IOA and IO ± A deposits. In many areas, Kiruna-type deposits are spatially and temporally associated with IOCG deposits, e.g., in the Chilean iron belt (Sillitoe, 2003), and in Missouri, United States (Day et al., 2016). The IOA and IOCG deposits form in regions of extension along subduction-related continental magmatic arcs, intracontinental orogenic collapse basins, or are associated with intracontinental anorogenic magmatism (Groves et al., 2010; Rieger et al., 2010). Here, a new genetic model presented (Figure 8) can explain both IOA and IO ± A mineralization systems in the Zanjan area.

This is consistent with the proposed model, in which IOA deposits represent the deeper roots of IOA/IOCG ore systems (e.g., Sillitoe, 2003; Day et al., 2016; Barra et al., 2017; Simon et al., 2018). The Zanjan monzonitic plutons are emplaced at 40.0 ± 1.4 Ma (Nabatian et al., 2014b) in an environment of lithospheric back-arc extension. The mineralization age of 39.99 ± 0.24 Ma (monazite included in apatite; Nabatian et al., 2014a) supports a close temporal and likely genetic relationship between magmatic processes and mineralization. The back-arc extension-related quartz monzonitic to quartz monzodioritic magmatism in the Zanjan area is responsible for magnetite ore mineralization. In our proposed model, IOA deposits such as, Sorkhe-Dizaj, Morvarid, Zaker, and Aliabad are inferred to have formed at deeper levels of magmatism. Simultaneously with magmatic emplacement, the proto-Fe–P oxide mineralization was generated with the formation of fine-grained magnetite and apatite disseminated iron ores. Subsequently, magmatic volatile-rich fluids (containing Fe, P, and rare earth elements) deposited iron oxide-apatite mineralization associated with diopside and minor actinolite at the end of this stage. Abundant magnetite and apatite mineralization started with magnetite-apatite stockworks, followed by the emplacement of vein-type ore bodies (main oxide mineralization) in fractures and fault zones. As the temperature and salinity of fluids decreased from Sorkhe-Dizaj to Zaker, abundant apatite decreased while the proportion of actinolite increased. At this time, the IO ± A Chore-Nab deposit formed at intermediate level above and close to the IOA deposits (Figure 8). The magmatic-hydrothermal fluid that precipitated magnetite and apatite within the deeper root zones of IOA/IOCG

systems (IOA deposits in the Sorkhe-Dizaj, Morvarid, Zaker, and Aliabad) will continue to transport significant amounts of dissolved Fe (plus Cu, Au) after IOA deposition (IOA-IOCG transition), finally forming hematite-rich IOCG deposits at shallower levels. It concludes that the IO ± A Chore-Nab deposit formed spatially between the deeper classic IOA and shallower IOCG deposits. In general, the Tarom-Hashtjin metallogenic province is dominated by iron oxide-only (IO ± A) and IOA deposits; IOCG (sensu stricto) deposits are absent. A major question thus remains regarding the Tarom-Hashtjin metallogenic province: despite the presence of sedimentary rocks such as, sandstone, siltstone, and mudstone, which are necessary for the formation of IOCG deposits (Williams et al., 2005), why have these deposits, which have a genetic connection with IOA deposits, not yet been discovered? However, evidence of the IOA-IOCG transition could potentially increase exploration success for IOCG deposits in the Tarom-Hashtjin metallogenic province in the future.

8. Concluding remarks

With the exception of numerous epithermal deposits, the Tarom-Hashtjin metallogenic province hosts iron oxide deposits associated with the Upper Eocene monzonitic magmatism. These types of mineralization are genetically related to the Eocene back-arc extension-related calc-alkaline magmatism. Field observations, mineralogy, fluid inclusion, and hydrothermal alteration data from iron oxide deposits in the Zanjan area reveal that the iron oxide mineralization at the Chore-Nab deposit exhibits various lines of evidence for the IOA and IOCG transition (IO ± A). Evaluation of mineralization and alteration, coupled with similar fluid evolution and magnetite geochemical signatures, suggests a distinct evolutionary history for magmatic-hydrothermal IOA deposits at the deeper levels and its change to transitional between IOA and IOCG at the Chore-Nab deposit (IO ± A) in the intermediate level close to IOA deposits.

The model described here, developed for deposits in the back-arc setting at the Tarom-Hashtjin metallogenic province, holistically explains the formation of IOA and IO ± A deposits as a combination of common igneous and magmatic-hydrothermal processes within the same area. These relationships enhance our understanding of fundamental geochemical processes that occur in other tectonic settings and may lead to the discovery of new IOA and IOCG ore systems.

Acknowledgments

This work was supported by the Iranian Mineral Processing Research Center (IMPRC) and Kharazmi University of Tehran, Iran. The authors would like to thank Mr. Torkashvand and Ebrahimi Fard for their assistance in the fieldwork and sample preparation. Additionally, the authors extend their sincere appreciation to Prof. David Lentz (University of New Brunswick, Canada) for careful English editing. The authors also acknowledge Editor Prof. Selahattin Kadir for his advice and dedicated editorial assistance. Furthermore, the authors would like to thank Dr. Necati Tüysüz and one anonymous reviewer for their advice and very helpful comments.

References

Aghazadeh M, Hou Z, Badrzadeh Z, Zhou L (2015). Temporal–spatial distribution and tectonic setting of porphyry copper deposits in Iran: Constraints from zircon U–Pb and molybdenite Re–Os geochronology. Ore Geology Reviews 70: 385–406. https://doi.org/10.1016/j.oregeorev.2015.03.003

Allen M, Jackson J, Walker R (2004). Late Cenozoic reorganization of the Arabia-Eurasia collision and the comparison of short-term and long-term deformation rates. Tectonics 23: TC2008. https://doi.org/10.1029/2003TC001530

Barra F, Reich M, Selby D, Rojas P, Simon AC et al. (2017). Unraveling the origin of the Andean IOCG clan: A Re-Os isotopes approach. Ore Geology Reviews 81: 62–78. https://doi.org/10.1016/j.oregeorev.2016.10.016

Barton MD (2014). Iron oxide (-Cu-Au-REE-P-Ag-U-Co) systems. Treatise on Geochemistry 13: 515–541. https://doi.org/10.1016/B978-0-08-095975-7.01123-2

Barton MD, Johnson DA (2004). Footprints of Fe-oxide (Cu-Au) systems. University of Western Australia, Centre for Global Metallogeny. Special Publication 33: 112–116.

Becker SP, Fall A, Bodnar RJ (2008). Synthetic fluid inclusions. XVII. PVTX properties of high salinity H2O–NaCl solutions (>30 wt% NaCl): application to fluid inclusions that homogenize by halite disappearance from porphyry copper and other hydrothermal ore deposits. Economic Geology 103: 539–554. https://doi.org/10.2113/gsecongeo.103.3.539

Bodnar RJ (1993). Revised equation and table for determining the freezing point depression of H2O-NaCl solutions. Geochimica et Cosmochimica Acta 57: 683–684. https://doi.org/10.1016/0016-7037(93)90378-A

Bonyadi Z, Davidson GJ, Mehrabi B, Meffre S, Ghazban F (2011). Significance of apatite REE depletion and monazite inclusions in the brecciated Se–Chahun iron oxide–apatite deposit, Bafq district, Iran: insights from paragenesis and geochemistry. Chemical Geology 281: 253–269.

Corriveau L, Montreuil JF, Potter EG (2016). Alteration facies linkages among iron oxide copper-gold, iron oxide-apatite, and affiliated deposits in the Great Bear magmatic zone, Northwest Territories, Canada. Economic Geology 111: 2045–2072. https://doi.org/10.2113/econgeo.111.8.2045

Daliran F (1990) The magnetite – apatite deposit of Mishdovan, east central Iran. An alkali rhyolite hosted "Kiruna-type" occurrence in the infracambrian Bafg metallotect; Ph.D. thesis, Univ. of Heidelberg. Geowiss. Abhandl. 37, 248 p.

Daliran F (1999) REE geochemistry of Bafg apatites: Implication for the genesis of Kiruna-type iron ores; Mineral deposits; processes to processing, Stanley et al. (Eds.) Balkema, Rotterdam, 631–634.

Daliran F (2002) Kiruna-type iron oxide-apatite ores and apatitites of Bafq district, Iran, with an emphasis on the REE geochemistry of their appetites. PGC Publishing, Linden Park, South Australia, 303–320.

Daliran F, Stosch HG, Williams P (2009) A review of the Early Cambrian magmatic and metasomatic events and their bearing on the genesis of the Fe oxide-REE-apatite deposits (IOA) of the Bafq District, Iran. In: Williams et al. (eds.) Smart science for exploration and mining: proceedings of the10th Biennial SGA Meeting, Townsville, Australia, 623–625.

Daliran F, Stosch HG, Williams P, Jamli H, Dorri MB (2010). Early Cambrian iron oxide-apatite-REE (U) deposits of the Bafq District, East Central Iran. In: Corriveau L, Mumin H (eds.) Exploring for iron oxide copper gold deposits: Canada and global analogues. Geological Association of Canada Short Course Notes 20: 143–155.

Day WC, Slack JF, Ayuso RA, Seeger CM (2016). Regional geologic and petrologic framework for Iron Oxide ± Apatite ± Rare Earth Element and Iron Oxide Copper-Gold deposits of the Mesoproterozoic St. Francois Mountains Terrane, Southeast Missouri, USA. Economic Geology 111 (8): 1825–1858. https://doi.org/10.2113/econgeo.111.8.1825

del Real I, Reich M, Simon AC, Deditius A, Barra F et al. (2021). Formation of giant iron oxide-copper-gold deposits by superimposed, episodic hydrothermal pulses. Communications Earth and Environment-Nature 2: 192. https://doi.org/10.1038/s43247-021-00265-w

Dupuis C, Beaudoin G (2011). Discriminant diagrams for iron oxide trace element finger printing of mineral deposit types. Mineralium Deposita 46: 319–335. https://doi.org/10.1007/s00126-011-0334-y

Edfelt A, Armstrong RN, Smith M, Martinsson O (2005). Alteration paragenesis and mineral chemistry of the Tjårrojåkka apatite–iron and Cu (–Au) occurrences, Kiruna area, northern Sweden. Mineralium Deposita 40 (4): 409–434. https://doi.org/10.1007/s00126-005-0005-y

Ghasemi Siani M, Lentz D (2022) Lithogeochemistry of various hydrothermal alteration types associated with precious and base metal epithermal deposits in the Tarom-Hashtjin metallogenic province, NW Iran: Implications for regional exploration. Journal of Geochemical Exploration 232. 106903. https://doi.org/10.1016/j.gexplo.2021.106903

Ghasemi Siani M, Lentz D, Nazarian M (2020). Geochemistry of igneous rocks associated with mineral deposits in the Tarom-Hashtjin metallogenic province, NW Iran: An analysis of the controls on epithermal and related porphyry-style mineralization. Ore Geology Reviews 126. https://doi.org/10.1016/j.oregeorev.2020.103753

Ghasemi Siani M, Mehrabi B, Azizi H, Wilkinson CM, Ganerod M (2015). Geochemistry and geochronology of the volcano-plutonic rocks associated with the Glojeh epithermal gold mineralization, NW Iran. Open Geosciences 7: 207–222.

Goldstein RH (2003). Petrographic analysis of fluid inclusions. In: Samson, I., Anderson, A., Marshall, D. (Eds.), Fluid Inclusions: Analysis and Interpretation. Mineralogical Association of Canada 32: 9–53.

Groves DI, Bierlein FP, Meinert LD, Hitzman MW (2010). Iron oxide copper–gold (IOCG) deposits through Earth history: implications for origin, lithospheric setting and distinction from other epigenetic iron oxide deposits. Economic Geology 105 (3): 641–654. https://doi.org/10.2113/gsecongeo.105.3.641

Hart CJR, Mair JL, Goldfarb RJ, Groves DI (2004). Source and redox controls on metallogenic variations in ore systems, Tombstone-Tungsten Belt, Yukon, Canada: Earth and Environmental Science Transactions of the Royal Society of Edinburgh 95 (2): 339–356. https://doi.org/10.1017/S0263593300001115

Hassanpour S, Alirezaei S, Selby D, Sergeev S (2015). SHRIMP zircon U–Pb and biotite and hornblende Ar–Ar geochronology of Sungun, Haftcheshmeh, Kighal, and Niaz porphyry Cu–Mo systems: evidence for an early Miocene porphyry-style mineralization in northwest Iran. International Journal of Earth Sciences 104: 45–59. https://doi.org/10.1007/s00531-014-1071-0

Heidarian H, Alirezaei S, Lentz D (2017). Chadormalu Kiruna-type magnetite-apatite deposit, Bafq district, Iran: Insights into hydrothermal alteration and petrogenesis from geochemical, fluid inclusion, and sulfur isotope data. Ore Geology Reviews 83: 42–63. https://doi.org/10.1016/j.oregeorev.2016.11.031

Hitzman MW (2000). Iron oxide–Cu–Au deposits: what, where, when, and why. In: Porter, T.M. (Ed.), Hydrothermal Iron Oxide Copper–Gold and Related Deposits: a Global Perspective. Australian Mineral Foundation, Adelaide, 9–25.

Hitzman MW, Oreskes N, Einaudi MT (1992). Geological characteristics and tectonic setting of Proterozoic iron oxide (Cu–U–Au–REE) deposits. Precambrian Research 58(1–4): 241–287. https://doi.org/10.1016/0301-9268(92)90121-4

Hitzman MW, Valenta RK (2005). Uranium in iron oxide-copper-gold (IOCG) systems. Economic Geology 100: 1657–1661. https://doi.org/10.2113/gsecongeo.100.8.1657

Jami M, Dunlop AC, Cohen DR (2007) Fluid inclusion and stable isotope study of the Esfordi apatite-magnetite deposit, central Iran. Econ Geol 102:1111–1128.

Kordian Sh, Mokhtari MAA, Kouhestani H, Veiseh S (2020). Geology, mineralogy, structure and texture, geochemistry and genesis of the Golestanabad iron oxide-apatite deposit (East of Zanjan) (in Persian). Journal of Economic Geology, 12: 299–325.

Kouhestani H, Mokhtari MAA, Qin KZ, Zhang XN (2020). Genesis of the Abbasabad epithermal base metal deposit, NW Iran: Evidences from ore geology, fluid inclusion and O-S isotopes. Ore Geology Reviews 126: 103752. https://doi.org/10.1016/j.oregeorev.2020.103752

Lecumberri Sanchez P, Steele MacInnis M, Bodnar RJ (2012). Numerical model to estimate trapping conditions of fluid inclusions that homogenize by halite disappearance. Geochimica et Cosmochimica Acta 92: 14–22. https://doi.org/10.1016/j.gca.2012.05.044

Mahdavi Akerdi M, Malekzadeh Shafaroudi A, Karimpour MH, Rahimi B, Santos JF (2021) Evidence of iron oxide-copper-gold mineralization in the Torud-Chahshirin Magmatic Belt, northern Iran: Insight from the Robaie area. Ore Geology Reviews 129. https://doi.org/10.1016/j.oregeorev.2020.103937

Mark G, Oliver NH, Williams PJ (2006). Mineralogical and chemical evolution of the Ernest Henry Fe oxide–Cu–Au ore system, Cloncurry district, northwest Queensland, Australia. Mineralium Deposita 40: 769–801. https://doi.org/10.1007/s00126-005-0009-7

Marschik R, Fontboté L (2001). The Candelaria–Punta del Cobre iron oxide Cu–Au (–Zn–Pb) deposits, Chile. Economic Geology 96: 1799–1826. https://doi.org/10.2113/96.8.1799

Mederer J, Moritz R, Zohrabyan SA, Vardanyan AV, Melkonyan RL et al. (2014). Base and precious metal mineralization in Middle Jurassic rocks of the Lesser Caucasus-a review of geology and metallogeny and new data from the Kapan, Alaverdi and Mehmana districts. Ore Geology Reviews 58: 185–207. https://doi.org/10.1016/j.oregeorev.2013.10.007

Mehrabi B, Ghasemi Siani M (2012). Intermediate sulfidation epithermal Pb-Zn-Cu (±Ag-Au) mineralization at Cheshmeh Hafez deposit, Semnan Province, Iran. Journal of Geological Society of India 80: 563–578. https://doi.org/10.1007/s12594-012-0177-x

Mehrabi B, Ghasemi Siani M, Goldfarb R, Azizi H, Ganerod N et al. (2016). Mineral assemblages, fluid evolution, and genesis of polymetallic epithermal veins, Glojeh district, NW Iran. Ore Geology Reviews 78: 41–57. https://doi.org/10.1016/j.oregeorev.2016.03.016

Mehrabi B, Ghasemi Siani M, Tale Fazel E (2015). Structural control on epithermal mineralization in the Troud-Chah Shirin Belt using Point Pattern and Fry Analyses, North of Iran. Geotectonics 49: 317–328. https://doi.org/10.1134/S001685211504007X

Mehrabi B, Ghasemi Siani M, Zhang R, Neubauer F, Lentz DR et al. (2021). Mineralogy, petrochronology, geochemistry, and fluid inclusion characteristics of the Dardvay skarn iron deposit, Sangan mining district, NE Iran. Ore Geology Reviews 134, https://doi.org/10.1016/j.oregeorev.2021.104146

Mehrabi M, Karimishahraki B, Banks D, Boyce A, Yardley BWD (2019). Hydrothermal iron oxide-Cu-Au (IOCG) mineralization at the Jalal-Abad deposit, northwestern Zarand, Iran. Ore Geology Reviews 106: 300–317. https://doi.org/10.1016/j.oregeorev.2019.01.019

Mirnejad H, Hassanzadeh J, Cousens BL, Taylor BE (2010). Geochemical evidence for deep mantle melting and lithospheric delamination as the origin of the inland Damavand volcanic rocks of northern Iran. Journal of Volcanology and Geothermal Research 198 (3–4): 288–296. https://doi.org/10.1016/j.jvolgeores.2010.09.014

Monteiro LVS, Xavier RP, de Carvalho ER, Hitzman MW, Johnson CA et al. (2008). Spatial and temporal zoning of hydrothermal alteration and mineralization in the Sossego iron oxide–copper–gold deposit, Carajás Mineral Province, Brazil: paragenesis and stable isotope constraints. Mineralium Deposita 43: 129–159. https://doi.org/10.1007/s00126-006-0121-3

Moritz R, Baker T (2019). Metallogeny of the Tethyan Orogenic Belt: From Mesozoic magmatic arcs to Cenozoic back-arc and postcollisional settings in southeast Europe, Anatolia, and the Lesser Caucasus: An Introduction. Economic Geology 114: 1227–1235. https://doi.org/10.5382/econgeo.4683

Nabatian G, Ghaderi M (2013). Oxygen isotope and fluid inclusion study of the Sorkhe-Dizaj iron oxide–apatite deposit, NW Iran. International Geology Review 55: 397–410. https://doi.org/10.1080/00206814.2012.713547

Nabatian G, Ghaderi M, Corfu F, Neubauer F, Bernroider M et al. (2014a). Geology, alteration, age, and origin of iron oxide–apatite deposits in Upper Eocene quartz monzonite, Zanjan district, NW Iran. Mineralium Deposita 49: 217–234. https://doi.org/10.1007/s00126-013-0484-1

Nabatian G, Ghaderi M, Daliran F, Rashidnejad Omran N (2013). Sorkhe-Dizaj iron oxide-apatite ore deposit in the Cenozoic Alborz–Azarbaijan magmatic belt, NW Iran. Resource Geology 63: 42–56. https://doi.org/10.1111/j.1751-3928.2012.00209.x

Nabatian G, Ghaderi M, Neubauer F, Honarmand M, Liu X et al. (2014b). Petrogenesis of Tarom high-potassic granitoids in the Alborz–Azarbaijan belt, Iran: Geochemical, U–Pb zircon and Sr–Nd–Pb isotopic constraints. Lithos 184–187: 324–345. https://doi.org/10.1016/j.lithos.2013.11.002

Nash JT (1976). Fluid inclusion petrology-data from porphyry copper deposits and application to exploration. United States Geological Survey 907-D, 16 p.

Niiranen T, Poutiainen M, Manttari I (2007). Geology, geochemistry, fluid inclusion characteristics, and U–Pb age studies on iron oxide–Cu–Au deposits in the Kolari region, northern Finland. Ore Geology Reviews 30: 75–105. https://doi.org/10.1016/j.oregeorev.2005.11.002

Niroomand S, Hassanzadeh J, Tajeddin HA, Asadi S (2018). Hydrothermal evolution and isotope studies of the Baghu intrusion-related gold deposit, Semnan province, north-central Iran Ore Geology Reviews 95: 1028–1048. https://doi.org/10.1016/j.oregeorev.2018.01.015

Oliver NHS, Cleverley JS, Mark G, Cleverley JS, Ord A et al. (2004). Modeling the role of sodic alteration in the genesis of iron oxide–copper–gold deposits, eastern Mount Isa block, Australia. Economic Geology 99: 1145–1176. https://doi.org/10.2113/gsecongeo.99.6.1145

Pollard PJ (2006). An intrusion-related origin for Cu–Au mineralization in iron oxide–copper–gold (IOCG) provinces. Mineralium Deposita 41: 179–187. https://doi.org/10.1007/s00126-006-0054-x

Reid A (2019). The Olympic Cu-Au Province, Gawler Craton: A review of the lithospheric architecture, geodynamic setting, alteration systems, cover successions and prospectivity. Minerals. https://doi.org/10.3390/min9060371

Rieger AA, Marschik R, Diaz M, Hlolzl S, Chiaradia M et al. (2010). The hypogene iron oxide-copper-gold mineralization in the Mantoverde district, northern Chile. Economic Geology 105 (7): 1271–1299. https://doi.org/10.2113/econgeo.105.7.1271

Roedder E (1984). Fluid Inclusions: Rev in Mineral 12, Miner Soc Am 644 p.

Shamanian GH, Hedenquist JW, Hattori KH, Hassanzadeh J (2004). The Gandy and Abolhassani epithermal prospects in the Alborz magmatic arc, Semnan Province, northern Iran. Economic Geology 99 (4): 691–712. https://doi.org/10.2113/99.4.691

Sillitoe RH (2003). Iron oxide–copper–gold deposits: an Andean view. Mineralium Deposita 38: 787–812. https://doi.org/10.1007/s00126-003-0379-7

Simon AC, Knipping J, Reich M, Barra F, Deditius AP (2018). Kiruna-type Iron Oxide-Apatite (IOA) and Iron Oxide Copper-Gold (IOCG) deposits formed by a combination of igneous and magmatic-hydrothermal processes: Evidence from the Chilean Iron Belt. SEG Special Publication 21: 89–114. https://doi.org/10.5382/SP.21.06

Smith MP, Coppard J, Herrington R, Stein H (2007). The geology of the Rakkurijarvi Cu–(Au) prospect, Norrbotten: a new IOCG deposit in Northern Sweden. Economic Geology 102 (3): 393–414. https://doi.org/10.2113/gsecongeo.102.3.393

Sterner SM, Hall DL, Bodnar RJ (1988). Synthetic fluid inclusions. V. Solubility relations in the system NaCl-KCl-H2O under vapor-saturated conditions. Geochimica et Cosmochimica Acta 52: 989–1005. https://doi.org/10.1016/0016-7037(88)90254-2

Stosch HG, Romer RL, Daliran F (2011). Uranium–lead ages of apatite from iron oxide ores of the Bafq District, East-Central Iran. Mineralium Deposita 46: 9–21. https://doi.org/10.1007/s00126-010-0309-4

Tale Fazel E, Mehrabi M, Ghasemi Siani M (2019). Epithermal systems of the Torud–Chah Shirin district, northern Iran: Ore-fluid evolution and geodynamic setting. Ore Geology Reviews 109: 253–275. https://doi.org/10.1016/j.oregeorev.2019.04.014

Torab FM, Lehmann B (2007) Magnetite–apatite deposits of the Bafq district, Central Iran: apatite geochemistry and monazite geochronology. Mineralogical Magazine 71: 347–363. https://doi.org/10.1180/minmag.2007.071.3.347

Verdel C, Wernicke BP, Hassanzadeh J, Guest B (2011). A Paleogene extensional arc flare-up in Iran. Tectonics 30. https://doi.org/10.1029/2010TC002809 (TC3008)

Williams P (2010). Classifying IOCG deposits. In: Exploring for Iron Oxide Copper–Gold Deposits: Canada and Global Analogues. Geological Association of Canada, Short Course Notes 20: 11–19.

Williams PJ, Barton MD, Johnson DA, Fontboté L, de Haller A et al. (2005). Iron oxide copper-gold deposits: geology, space-time distribution, and possible modes of origin. In: 100th Anniversary of Economic Geology 371–405. https://doi.org/10.5382/AV100.13

Williams PJ, Pollard PJ (2003). Australian Proterozoic iron oxide–Cu–Au deposits: An overview with new metallogenic and exploration data from the Cloncurry district, northwest Queensland. Exploration and Mining Geology 10 (3): 191–213. https://doi.org/10.2113/0100191

Supplementary material

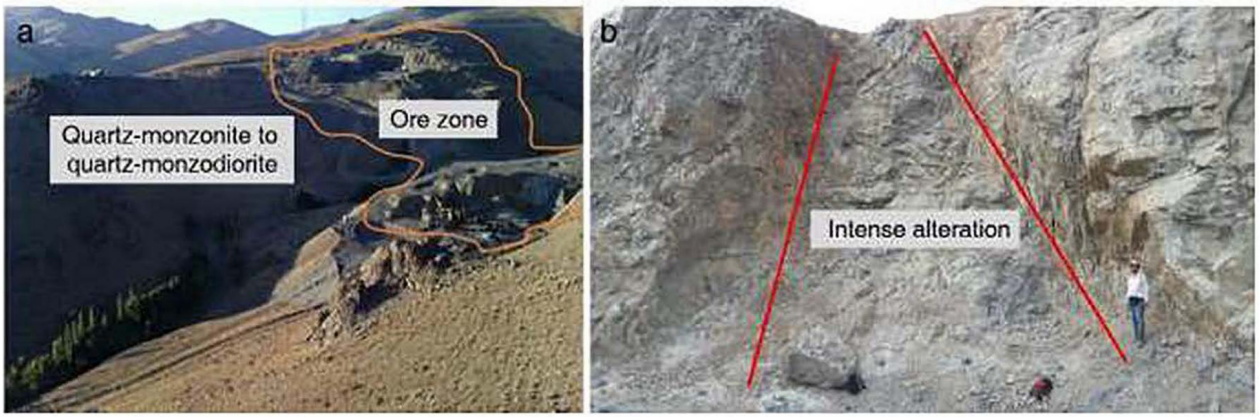

Supplementary Figure 1. a) Ore zones in the quartz monzonite to quartz monzodiorite host intrusion, and b) intense alteration zone around fractures and faults.

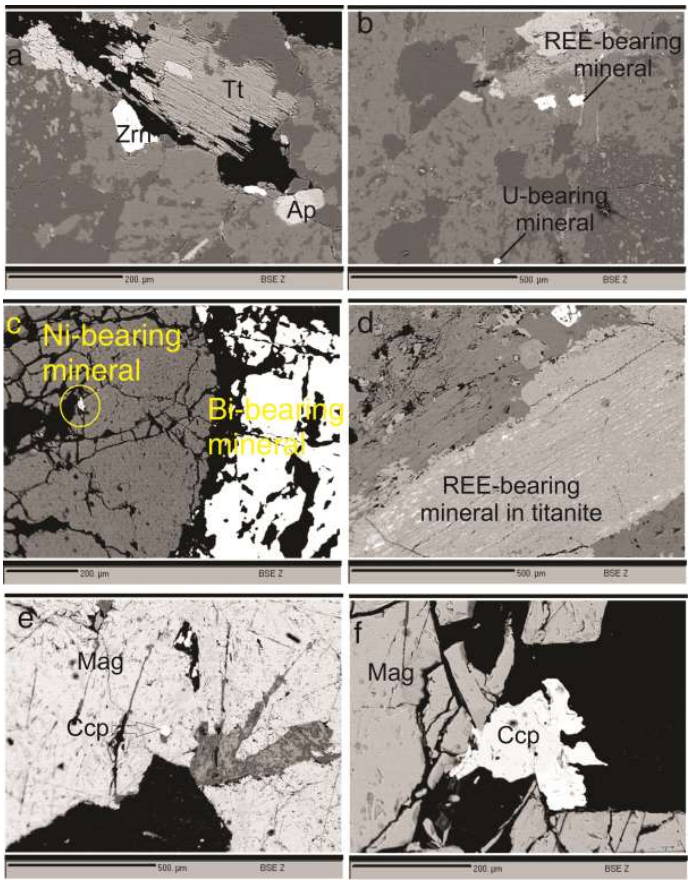

Supplementary Figure 2. a) EPMA back-scattered electron images of zircon, titanite and apatite; b) REE-bearing and U-bearing minerals in the vein texture; c) Ni and Bi-bearing minerals associated with pyrite in the vein texture; d) REE-bearing minerals (white) in the titanite, and e and f) magnetite and chalcopyrite in the vein-type and disseminated ore textures, respectively. Tt, titanite; Zrn, zircon; Ap, apatite; Mag, magnetite; Ccp, chalcopyrite.

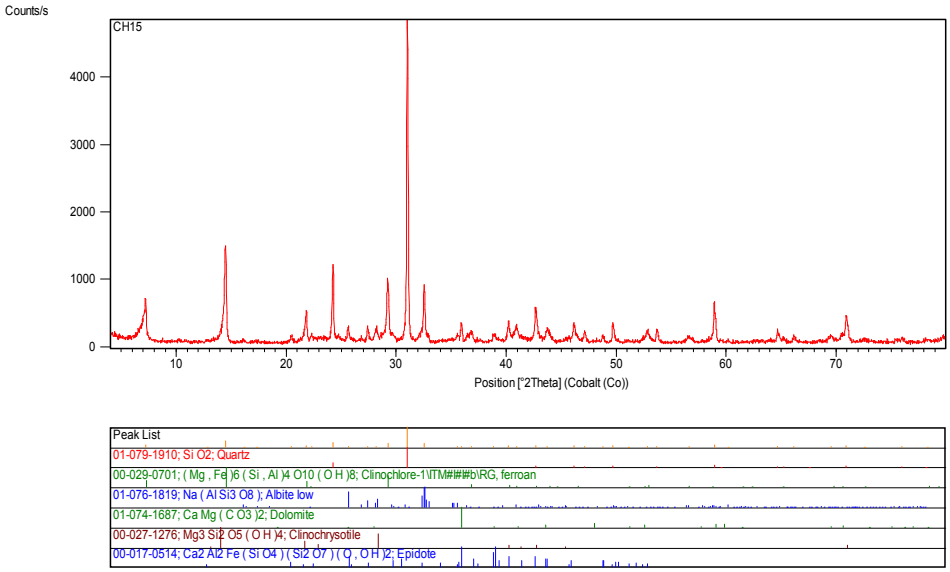

Supplementary Figure 3. XRD patterns showing dolomite, clinocrysotile, quartz, chlorite-epidote, and albite at zones of propylitic alteration.

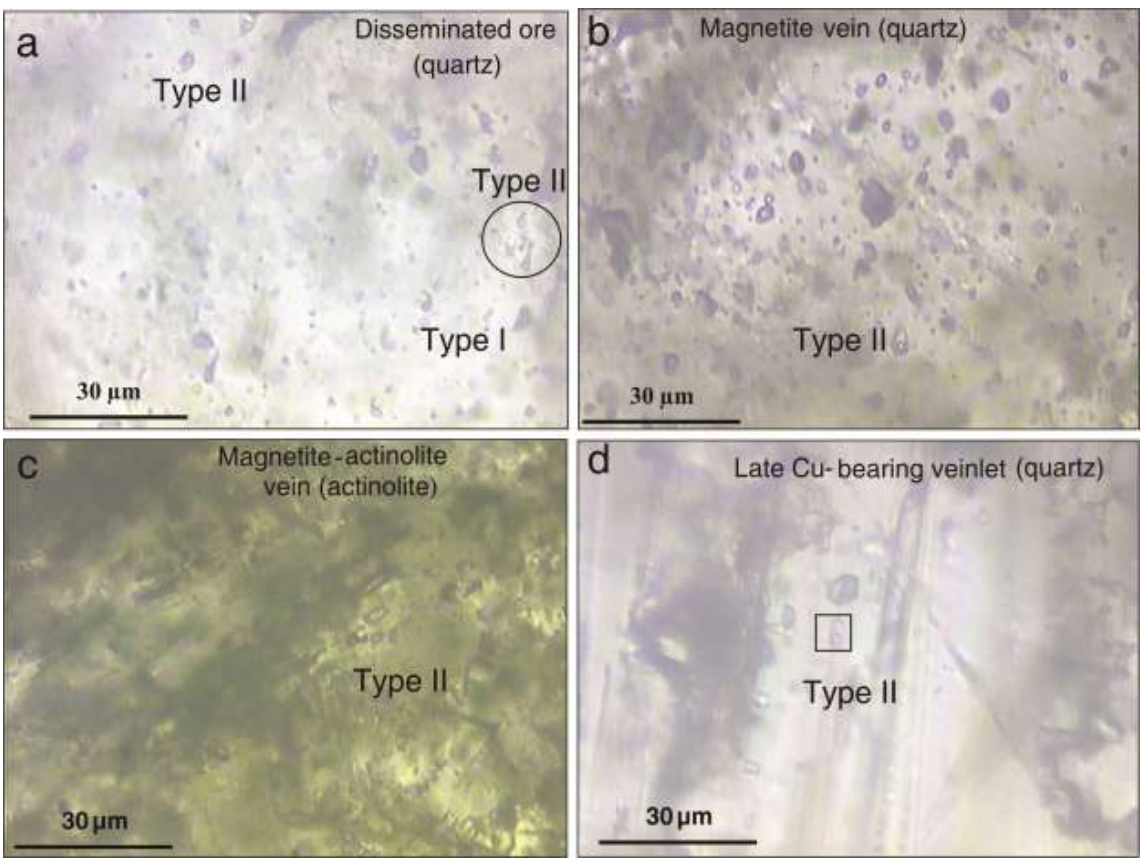

Supplementary Figure 4. Photomicrographs of representative fluid inclusions in the Chore-Nab deposit. a) Type LV and LVS fluid inclusion assemblages in quartz of the disseminated ore texture; b) types LV fluid inclusion assemblage in quartz of the magnetite ore veins; c) type LV inclusions in actinolite of the magnetite-actinolite vein, and d) type LV inclusions in quartz of the late chalcopyrite veinlet.

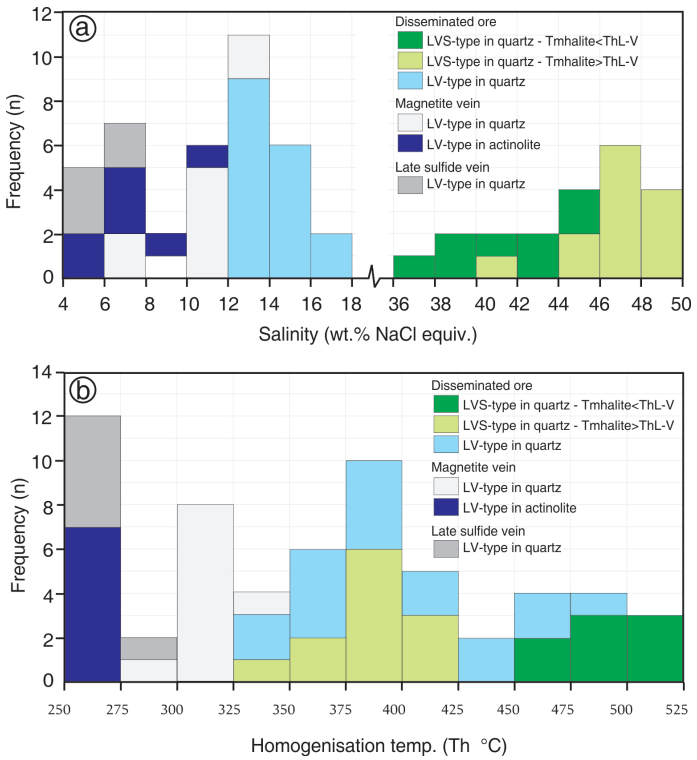

Supplementary Figure 5. a) Histograms of final homogenization temperatures (Th), and b) histograms of salinities (wt.% NaCl equiv.) for fluid inclusions at the Chore-Nab deposit.

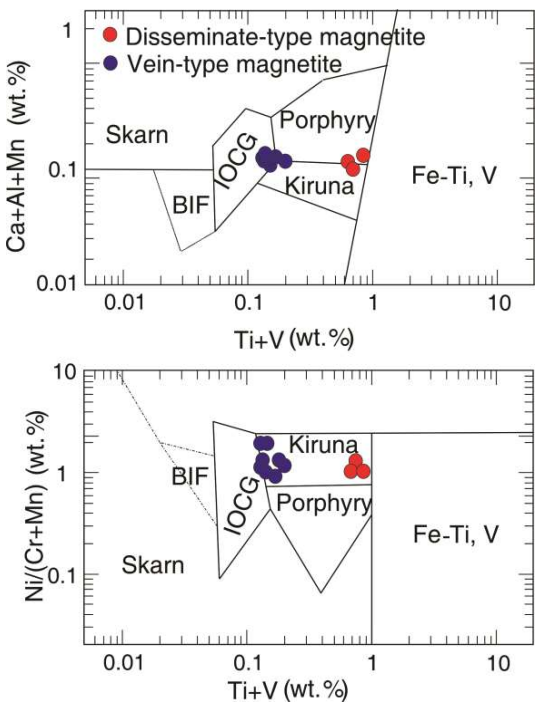

Supplementary Figure 6. Plots of V+Ti versus Ni/(Cr+Mn) and Ca+Al+Mn of magnetite in the Chore-Nab deposit (after Dupuis and Beaudoin, 2011).